Available online at www.sciencedirect.com

ScienceDirect

Geochimica et Cosmochimica Acta 199 (2017) 164–184

Geochimica et Cosmochimica Acta

www.elsevier.com/locate/gca

Water mass circulation and weathering inputs in the Labrador Sea based on coupled Hf–Nd isotope compositions and rare earth element distributions

Alexandra Filippova [a,*], Martin Frank [a], Markus Kienast [b], Jörg Rickli [c], Ed Hathorne [a], Igor M. Yashayaev [d], Katharina Pahnke [e]

[a] GEOMAR Helmholtz Centre for Ocean Research Kiel, Kiel, Germany
[b] Dalhousie University, Halifax, Canada
[c] ETH Zurich, Institute of Geochemistry and Petrology, Switzerland
[d] Bedford Institute of Oceanography, NS, Canada
[e] Max Planck Research Group for Marine Isotope Geochemistry, Institute for Chemistry and Biology of the Marine Environment (ICBM), Carl von Ossietzky University Oldenburg, 26129 Oldenburg, Germany

Received 25 January 2016; revised 11 November 2016; accepted in revised form 14 November 2016; Available online 21 November 2016

Abstract

The Labrador Sea is one of the key areas for deep water formation driving the Atlantic thermohaline circulation and thus plays an important role in Northern Hemisphere climatic fluctuations. In order to better constrain the overturning processes and the origins of the distinct water masses, combined dissolved Hf–Nd isotopic compositions and rare earth element (REE) distribution patterns were obtained from four water depth profiles along a section across the Labrador Sea. These were complemented by one surface sample off the southern tip of Greenland, three shallow water samples off the coast of Newfoundland, and two deep water samples off Nova Scotia.

Although light REEs are markedly enriched in the surface waters off the coast of Newfoundland compared to north Atlantic waters, the REE concentration profiles are essentially invariant throughout the water column across the Labrador Sea. The hafnium concentrations of surface waters exhibit a narrow range between 0.6 and 1 pmol/kg but are not significantly higher than at depth.

Neodymium isotope signatures (εNd) vary from unradiogenic values between −16.8 and −14.9 at the surface to more radiogenic values near −11.0 at the bottom of the Labrador Sea mainly reflecting the advection of the Denmark Strait Overflow Water and North East Atlantic Deep Water, the signatures of which are influenced by weathering contributions from Icelandic basalts. Unlike Nd, water column radiogenic Hf isotope signatures (εHf) are more variable representing diverse weathering inputs from the surrounding landmasses. The least radiogenic seawater εHf signatures (up to −11.7) are found in surface waters close to Greenland and near the Canadian margin. This reflects the influence of recirculating Irminger Current Waters, which are affected by highly unradiogenic inputs from Greenland. A three to four εHf unit difference is observed between Denmark Strait Overflow Water (εHf ∼ −4) and North East Atlantic Deep Water (εHf ∼ −0.1), although their source waters have essentially the same εNd signature. This most likely reflects different weathering signals of hafnium delivered to Denmark Strait Overflow Water and North East Atlantic Deep Water (incongruent weathering of old rocks from Greenland versus basaltic rocks from Iceland). In addition, the εHf data resolve two layers within the main body of Labrador Sea Water not visible in the εNd distribution, which are shallow Labrador Sea Water (εHf ∼ −2) and deep Labrador Sea Water (εHf ∼ −4.5). The latter layer was formed between the late 1980's and mid 1990's during the last cold state of the

* Corresponding author.
E-mail address: afilippova@geomar.de (A. Filippova).

http://dx.doi.org/10.1016/j.gca.2016.11.024

Labrador Sea and underwent substantial modification since its formation through the admixture of Irminger Water, Iceland Slope Water and North East Atlantic Deep Water, which is reflected in its less radiogenic εHf signature. The overall behavior of Hf in the water column suggests its higher sensitivity to local changes in weathering inputs on annual to decadal timescales. Although application of Hf isotopes as a tracer for global water mass mixing is complicated by their susceptibility to incongruent weathering inputs they are a promising tracer of local processes in restricted basins such as the Labrador Sea.

Keywords: The Labrador Sea; Hafnium; Neodymium; Seawater; Circulation

1. INTRODUCTION

Combined radiogenic Hf and Nd isotope compositions are a powerful tool to trace present and past ocean circulation and changes in weathering inputs (Bayon et al., 2006, 2009; Godfrey et al., 2009; Rickli et al., 2009, 2010; Chen et al., 2012; Stichel et al., 2012a,b) but the exact mechanisms controlling their behavior and distribution in seawater, in particular those of Hf isotopes, are still not well constrained. Due to very small differences in the abundance of the radiogenic isotopes (^{176}Hf, ^{143}Nd), the hafnium and neodymium isotope ratios of interest (^{176}Hf/^{177}Hf or ^{143}Nd/^{144}Nd) are normally expressed in epsilon units as deviations from the Chondritic Uniform Reservoir corresponding to 0.512638 for Nd (Jacobsen and Wasserburg, 1980) and 0.282785 for Hf (Bouvier et al., 2008).

$$\varepsilon\mathrm{Hf}\text{ or }\varepsilon\mathrm{Nd} = [R_{SAMPLE}/R_{CHUR} - 1] * 10000,$$

where R reflects ^{176}Hf/^{177}Hf and ^{143}Nd/^{144}Nd, respectively.

The neodymium isotope composition in seawater has been studied for many decades (since the late 70's) resulting in a large data set of εNd signatures of different water masses in the global ocean ranging from −26.6 to +2.7 (Grasse et al., 2012; Lacan et al., 2012; Fröllje et al., 2016). Clear and well resolved εNd signatures of different water masses in the ocean reflect weathering inputs from rocks different in age and type in their source areas. The average residence time of Nd is on the order of 400–1000 years (Arsouze et al., 2009; Rempfer et al., 2011). Given that the Nd isotope signatures generally covary with salinity and nutrient content of deep waters in the modern ocean, they have also been used as a tracer for past water mass mixing and ocean circulation based on seawater-derived Nd isotope signatures extracted from sediments (cf. Frank, 2002; Goldstein and Hemming, 2003; Piotrowski et al., 2005). Neodymium isotopes are generally not influenced by fractionation during weathering processes (Goldstein et al., 1984) with evidence for limited incongruent weathering of Nd isotopes in some high latitude glacial weathering environments (Öhlander et al., 2000; Andersson et al., 2001).

In contrast, the applicability of Hf isotopes for the reconstruction of water mass mixing is complicated by a strong incongruent weathering effect on Hf isotopes resulting in a relatively low variability between different water masses (van de Flierdt et al., 2007; Rickli et al., 2009; Stichel et al., 2012a,b). However, seawater Hf isotopic compositions appear to be sensitive to changing continental weathering conditions implying that they are a valuable tool to monitor such changes (van de Flierdt et al., 2002). Early studies on the behavior of Hf and its isotopic distribution in seawater were based on data of slowly accumulating ferromanganese crusts and nodules (Albarède et al., 1998; David et al., 2001; van de Flierdt et al., 2002, 2004a,b; Bau and Koshinsky, 2006). Direct measurements of the Hf isotope composition in seawater are, however, still scarce. Low concentrations of Hf (0.04–1.47 pmol kg^{-1}) (Godfrey et al., 1996; McKelvey and Orians, 1998) in comparison to Nd (15–45 pmol kg^{-1}) (Goldstein and Hemming, 2003) make these measurements analytically challenging. Isotopic compositions of Hf in seawater are available for the Atlantic Ocean (Godfrey et al., 2009; Rickli et al., 2009, 2010), the Southern Ocean (Stichel et al., 2012a,b; Rickli et al., 2014), the Pacific Ocean (Zimmermann et al., 2009b), the Arctic Ocean (Zimmermann et al., 2009a), and the central Baltic Sea (Chen et al., 2013). Global open ocean εHf signatures range from −5.7 to +10 (Godfrey et al., 2009; Rickli et al., 2009, 2010, 2014; Zimmermann et al., 2009a,b; Stichel et al., 2012a,b; Chen et al., 2013); all εHf values are given relative to the new CHUR value of 0.282785 from Bouvier et al., 2008).

Hafnium and Nd isotope compositions are closely correlated in continental rocks and oceanic basalts, which is a consequence of their similar behavior during magmatic processes. This results in a well-constrained linear trend in a plot of εHf against εNd known as the "mantle-crust array" or "terrestrial array" ($\varepsilon\mathrm{Hf} = 1.55 * \varepsilon\mathrm{Nd} + 1.21$, Vervoort et al., 2011). Studies on ferromanganese crusts already suggested that seawater samples form a separate well-defined trend, which deviates from the terrestrial array and is referred to as the "seawater array" ($\varepsilon\mathrm{Hf} = 0.62 * \varepsilon\mathrm{Nd} + 7.38$, Godfrey et al., 1997; Albarède et al., 1998; David et al., 2001). For a given εNd the εHf values are more radiogenic than the terrestrial array. The direct measurements of seawater carried out over the last decade confirmed the existence of the offset seawater array. One of the possible explanations for this offset is the difference in the behavior of Nd and Hf isotopes during continental weathering. Large fractions of the rock-hosted unradiogenic Hf are trapped in zircons highly resistant to weathering. During weathering this leads to preferential release of highly radiogenic Hf from the non-zircon portion of the rocks to river waters and eventually to the ocean (Bayon et al., 2006; Rickli et al., 2013), which is referred to as the "zircon effect" (Patchett et al., 1984). However, isotopic mass balance calculations show that the seawater offset cannot be solely explained by the zircon effect (Chen et al.,

2011). Instead, it has been proposed that weathering of minerals with high Lu/Hf such as garnet, apatite and sphene also play an important role (Barfod et al., 2003; Bayon et al., 2009; Godfrey et al., 2009; Chen et al., 2011).

Similar to Nd, the contribution of hydrothermal Hf to seawater is thought to be negligible based on the currently available data. This, however, still remains to be proven by direct measurements of Hf in hydrothermal solutions (van de Flierdt et al., 2004a,b; Bau and Koshinsky, 2006; Firdaus et al., 2011). Pettke et al. (2002) evaluated the role of aeolian inputs as a source of radiogenic Hf to seawater and found it to be of minor importance. Later Rickli et al. (2010) observed significant release of Hf from Saharan dust to surface waters of the Eastern Atlantic Ocean. Once dissolved in seawater, the estimates of the residence time of Hf show a large range between a few hundred and several thousand years (Godfrey et al., 1996; Firdaus et al., 2008; Rickli et al., 2009), which reflects the different approaches of estimation and our still limited understanding of Hf behavior in seawater.

Here we present the first systematic study of combined dissolved Hf and Nd isotope compositions and REE distribution patterns in the Labrador Sea. The aim of this study is to trace the mechanisms by which deep water masses obtain their radiogenic isotope signature and to evaluate the applicability of Hf isotopes as a tracer for water mass mixing on relatively short time and length scales in the light of the new data.

2. MATERIALS AND METHODS

2.1. Seawater

Twenty-six 20 L seawater samples were collected during an expedition in May 2013 on board of CCGS Hudson (Fig. 1, Table 1). Four full water depth profiles were collected across the Labrador Sea along the AR7W transect. Station 8.5 is the station closest to the coast with a water depth of 1702 m, located over the Labrador Sea slope and sampling the waters of the Labrador Current (LC, Table 2). The depth of the station is not sufficient to sample North East Atlantic Deep Water (NEADW) and Denmark Strait Overflow Water (DSOW). Stations 13.6 and 15.5 are located on the Labrador slope at a depth of about 3560 m, which is deep enough to sample all water masses present in the Labrador Sea. Station 17.5 is the deepest station sampled (~3620 m), located in the central part of the Labrador Sea. Each station was sampled at five different depths, covering the main water masses in the Labrador Sea. Station 28, located at the southern tip of Greenland, is a shallow station (~100 m). The station samples waters coming from the Arctic and waters of Irminger Sea origin. Shallow stations BIL02, BIL04 and BIL06 (depth less than 300 m) were sampled along the Belle Isle line, in close proximity to the coast of Newfoundland. Additionally, two deep water samples HL11 and HL08, representing lower North Atlantic Deep Water (NADW), were collected along the extended Halifax line on the way out of the Labrador Sea, off the coast of Nova Scotia, above the Nova Scotian slope.

2.2. Hydrography

The Labrador Sea plays an important role in controlling the strength of the Atlantic thermohaline circulation (Azetsu-Scott et al., 2003). As one of the regions of deep water formation contributing to NADW and as the last recipient of warm saline waters advected from the tropical Atlantic, the Labrador Sea has had a significant impact on the global climate and its variability on seasonal to multi-millennial timescales (Yashayaev et al., 2015) and vice versa. Temperatures and salinities recorded in May 2013 in the Labrador Sea were higher than previously recorded between 1994 and 2008 suggesting that warming had already reached the deepest layers of the Labrador Sea (Yashayaev and Loder, 2009, 2016).

The Labrador Sea is characterized by a cyclonic circulation (Lazier and Wright, 1993) formed by the LC, the West Greenland Current (WGC) and its underlying current, extending to the Deep Western Boundary Current (DWBC) (Fig. 1) (Azetsu-Scott et al., 2003). This cyclonic circulation is bounded by the North Atlantic Current (NAC) on its southeastern margin (Azetsu-Scott et al., 2003; Yashayaev and Clark, 2006; Yashayaev et al., 2015).

Surface waters on the Labrador shelves and slopes down to a depth of about 200 m are relatively warm and fresh ($T > 2.8$ °C, $S < 34.8$) and are formed by mixing of WGC, LC, Irminger Current (IC), NAC and large fresh water inputs from land (Lazier et al., 2002). Spreading offshore, these waters create a distinct body between 100 and 200 m water depth (Lazier et al., 2002) and produce alongshore currents (Csanady, 1976, 1978; Smith and Schwing, 1990). The presence of LC waters, that can propagate up to depths of 1500 m (deep LC) on the southeastern Labrador shelf and slope was detected at the shallow stations (BIL02; BIL04; BIL06) along the Belle Isle line. The position of the stations lies in the pathway of cold and fresh waters, flowing from the Hudson Strait and Baffin Bay along the Canadian shelf, which is consistent with the cold temperatures and low salinities at stations BIL02, BIL04 ($T \sim -1.2$ °C to -1.4 °C; $S \sim 32.91$–32.99, Fig. 2). In addition, they may have been influenced by admixture of waters intruding from the coast through the Belle Isle Strait (Fig. 1). Waters sampled at station BIL06, located further offshore, are slightly warmer and saltier ($T \sim 0$ °C, $S \sim 33.62$).

The hydrographic properties of the water collected at station 28 on the Greenland shelf from a depth of 107 m (7.5 ml/l oxygen, 1.85 °C and a relatively low salinity of 34.07) are consistent with waters of polar origin transported by the WGC (continuation of the East Greenland current). However, temperature and salinity increase with depth at station 28, indicating the presence of waters originating from the Irminger Current (IC, Fig. 1), which flows in from the Irminger Sea and propagates as a tongue of saltier, warmer waters into the Labrador Sea at depths of 300–800 m (Reynaud et al., 1995; Fogelqvist et al., 2003). Its deeper parts contain Iceland Slope Waters (ISW) (Yashayaev et al., 2008). The temperature and salinity signal of this current is also detectable at the northern and southern margin of the Labrador Sea but is more pronounced on the Green-

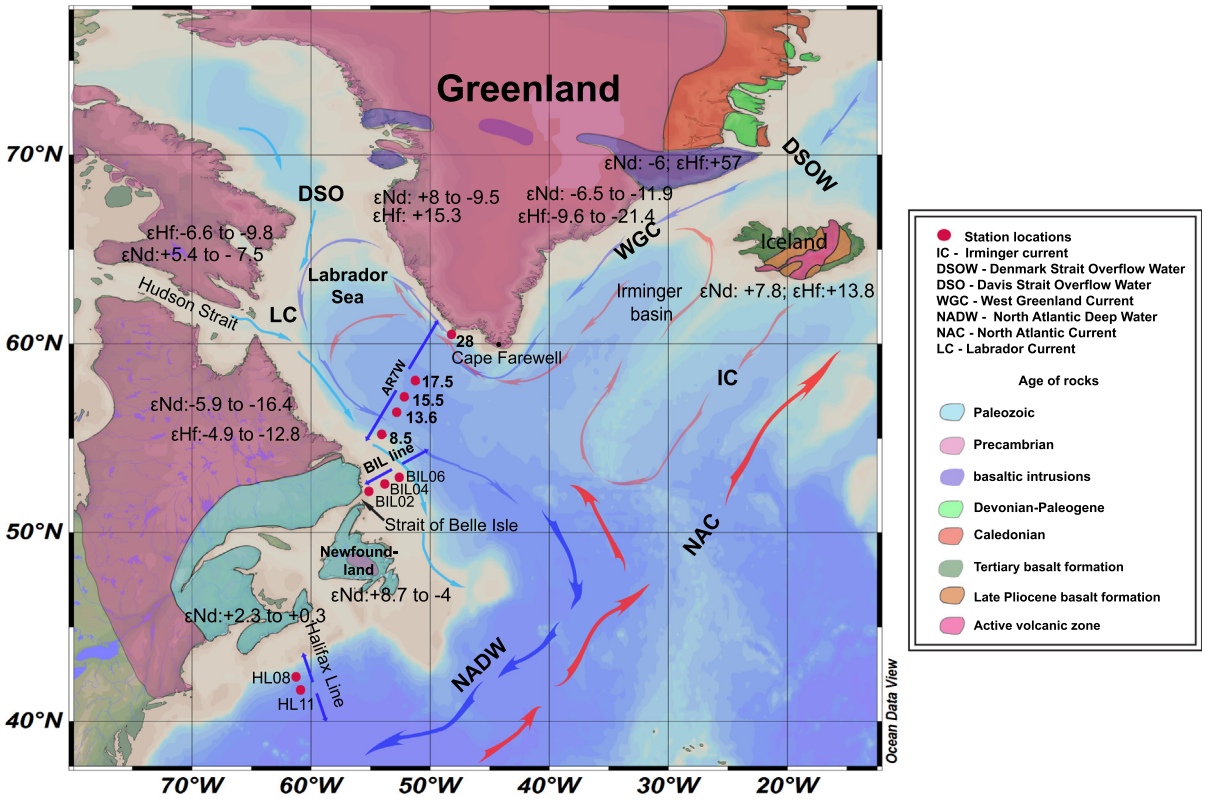

Fig. 1. Schematic map of the study area. Blue arrows represent cold deep currents and red arrows denote warm surface currents. Red dots indicate the positions of the stations occupied during CCGS Hudson Cruise 2013. A schematic representation of the geology of the surrounding landmasses is shown and includes average εHf and εNd values of the rocks. For full ranges of the values, please refer to original publications (Gerasimovsky et al., 1975; Zindler et al., 1982; Swinden et al., 1990; Stern et al., 1994; Camire et al., 1995; Skulski and Percival, 1996; La Fleche et al., 1998; Maclachlan and Dunning, 1998; Maclachlan et al., 1998; Nowell et al., 1998; Salters and White, 1998; Blichert-Toft and Arndt, 1999; Fitton et al., 2000; Goodenough et al., 2002; Stracke et al., 2003; West et al., 2004; Gaffney et al., 2007; Kitagawa et al., 2008; Tappe et al., 2008; Hoffmann et al., 2010; Jackson et al., 2010; Peate et al., 2010; Chekol et al., 2011; Koornneef et al., 2012; Szilas et al., 2012; Szilas et al., 2013; Minifie et al., 2013; Rizo et al., 2013; Manning and Thirlwall, 2014). Figure was created with ODV software (Schlitzer, 2015). (For interpretation of the references to colour in this figure legend, the reader is referred to the web version of this article.)

land side because eddy formation and recirculation dilute these waters along their pathway around the Labrador Sea (Yashayaev and Clark, 2006). At the southern margin of the Labrador Sea these waters have been sampled in the upper few hundred meters at station 8.5, at densities between 27.69 and 27.71 kg/m^3 (normalized to zero pressure at surface layer) (Fig. 2B, D).

The penetration depths of newly formed Labrador Sea Water (LSW) (from 900 up to 2400 m) depend on the intensity of cold, northwesterly winds blowing from Canada over the surface of the Labrador Sea and on the severity of winters in previous years (Yashayaev and Clark, 2006). In addition, stratification of the affected water column before and at the time of each convective event also plays a role. The 2012/2013 wintertime convection of the Labrador Sea was moderately strong producing mixed layer depths varying between 1300 and 1500 m that were not uniformly distributed across the Labrador Sea. The presence of shallow LSW (SLSW) at all stations is clearly marked by salinities of 34.85–34.87 and temperatures around 3.6 °C (Fig. 2B), covering the density range from 27.71 to up to 27.725 kg/m^3. Oxygen concentrations of these waters are relatively high at 6.5–6.6 ml/l (Fig. 2D).

A gradual increase in salinities to up to 34.91–34.92 at all stations (Fig. 2 B) reaching densities near 27.75 kg/m^3 (Fig. 2D) likely indicates the presence of old deep LSW (DLSW) produced between 1987 and 1994 during the most recent cold state of the Labrador Sea when deep convection reached down to 2400 m. In subsequent years, convection only reached to shallower depths, and this layer of higher density, salinity and temperature formed through admixture with IW, and ISW became isolated and by the time of sampling in 2013 had lost most of its volume (Yashayaev et al., 2008).

The relatively salty water mass below LSW reaching a density of 27.8 kg/m^3 recorded at stations 13.6, 15.5 and 17.5 is the North East Atlantic Deep Water (NEADW), the core of which is associated with a deep salinity maximum at 2500–3000 meters ($S \sim 34.92$, $\sigma \sim 27.85$–27.87, oxygen concentrations of ~6.2 ml/l, Fig. 2B, D) (Yashayaev, 2007). The sample from 2500 m water depth along the Halifax line (st. HL08) has temperature charac-

Table 1
Information about each station: longitude, latitude, temperature, salinity, oxygen and density, together with Hf and Nd isotope signatures and concentrations. Both internal and external errors of the measurements are shown.

Station	Depth of station [m]	Latitude [N]	Longitude [W]	Device	Depth [m]	Water mass	Salinity	T [°C]	σ [kg/m^3]	O_2 [ml/l]	$^{143}Nd/^{144}Nd$	εNd	Internal error 2S.E.M.	External error 2S.D.	$^{143}Nd/^{144}Nd$	Second run εNd	External error 2S.D.	Nd [pmol/kg]	$^{176}Hf/^{177}Hf$	εHf	Internal error 2S.E.M.	External error 2S.D.	Hf [pmol/kg]
8.5		55.19	−54.06	CTD	150	Surface	34.66	3.35	27.58	7.09	0.511811 ± 6	−15.8	0.3	0.4				20.2	0.282704 ± 16	−2.9	0.6	0.5	0.70
8.5		55.19	−54.06	CTD	400	IW	34.89	3.94	27.71	6.50	0.511891 ± 18	−14.0	0.3	0.4				18.0	0.282551 ± 13	−8.3	0.5	0.5	0.79
8.5	1702	55.19	−54.06	CTD	750	SLSW	34.85	3.48	27.72	6.61	0.511885 ± 12	−14.3	0.3	0.4				18.6	0.282662 ± 11	−4.3	0.4	0.5	0.67
8.5		55.19	−54.06	CTD	1050	DLSW	34.90	3.65	27.74	6.26	0.511908 ± 18	−13.7	0.3	0.4				18.0	0.282670 ± 18	−4.1	0.6	0.6	0.83
8.5		55.19	−54.06	CTD	1500	DLSW	34.91	3.56	27.76	6.17	0.511911 ± 12	−13.7	0.3	0.4				18.0	0.282723 ± 19	−2.2	0.7	0.6	1.03
13.6		56.37	−52.85	CTD	100	Surface	34.67	3.25	27.59	6.97	0.511775 ± 8	−16.4	0.3	0.4				19.6	0.282564 ± 11	−7.8	0.4	0.6	1.02
13.6		56.37	−52.85	CTD	1000	SLSW	34.86	3.54	27.72	6.62	0.511850 ± 6	−14.6	0.3	0.4				18.4	0.282688 ± 12	−3.4	0.4	0.6	0.73
13.6	3560	56.37	−52.85	CTD	1700	DLSW	34.92	3.54	27.76	6.07	0.511889 ± 16	−14.0	0.3	0.4				18.0	0.282646 ± 13	−4.9	0.5	0.6	0.80
13.6		56.37	−52.85	CTD	2400	NEADW	34.92	2.95	27.82	6.14	0.511965 ± 4	−12.6	0.3	0.4				16.7	0.282681 ± 16	−3.7	0.6	0.6	1.13
13.6		56.37	−52.85	CTD	3360	DSOW	34.90	1.76	27.91	6.45	0.512044 ± 10	−11.2	0.3	0.4				18.5	0.282777 ± 21	−0.3	0.7	0.6	0.96
15.5		57.17	−52.01	CTD	80	Surface	34.60	3.39	27.53	7.27	0.511803 ± 15	−16.0	0.5	0.3	0.511639 ± 8	−16.8*	0.5	19.2	0.282737 ± 13	−1.7	0.4	0.6	1.02
15.5		57.17	−52.01	CTD	1000	SLSW	34.87	3.60	27.72	6.48	0.511879 ± 20	−14.3	0.4	0.4				18.5	0.282731 ± 18	−1.9	0.6	0.6	1.64
15.5	3574	57.17	−52.01	CTD	1700	DLSW	34.92	3.48	27.77	6.08	0.511924 ± 8	−13.7	0.3	0.4				19.3	0.282711 ± 17	−2.6	0.6	0.6	1.21
15.5		57.17	−52.01	CTD	2300	NEADW	34.92	3.00	27.82	6.14	0.511969 ± 12	−12.7	0.3	0.4				16.6	0.282779 ± 17	−0.2	0.6	0.6	0.77
15.5		57.17	−52.01	CTD	3512	DSOW	34.90	1.49	27.93	6.57	0.512051 ± 20	−11.0	0.4	0.4				18.1	0.282653 ± 13	−4.7	0.5	0.6	3.95
17.5		58.01	−51.10	CTD	80	Surface	34.79	3.96	27.62	7.15	0.511851 ± 26	−14.9	0.5	0.4				19.7	0.282738 ± 17	−1.7	0.6	0.6	0.62
17.5		58.01	−51.10	CTD	1000	SLSW	34.85	3.48	27.71	6.61	0.511884 ± 13	−14.4	0.5	0.3	0.511751 ± 9	−14.5*	0.5	18.6	0.282748 ± 15	−1.3	0.5	0.6	0.73
17.5	3620	58.01	−51.10	CTD	2000	DLSW	34.92	3.49	27.77	6.09	0.511886 ± 14	−14.2	0.3	0.4				19.7	0.282659 ± 18	−4.5	0.6	0.6	0.79
17.5		58.01	−51.10	CTD	3000	NEADW	34.92	2.58	27.85	6.20	0.511996 ± 24	−12.1	0.5	0.4				15.2	0.282793 ± 13	0.3	0.4	0.6	0.73
17.5		58.01	−51.10	CTD	3670	DSOW	34.90	1.48	27.92	6.66	0.512024 ± 12	−11.6	0.3	0.4				16.8	0.282694 ± 16	−3.2	0.6	0.6	0.83
28	107	60.59	−48.23	CTD	100	IW	34.07	1.85	27.23	7.49	0.511839 ± 21	−15.3	0.4	0.3	0.511699 ± 10	−15.7*	0.5	26.0	0.282455 ± 12	−11.7	0.4	0.5	0.84
BIL02	147	52.20	−55.19	CTD	50	Surface	32.91	−1.49	26.48	7.91	0.511311 ± 8	−25.4	0.1	0.4	0.511177 ± 7	−25.9	0.3	48.2	0.282524 ± 11	−9.2	0.4	0.6	1.13
BIL04	199	52.56	−53.91	CTD	50	Surface	32.99	−1.27	26.53	7.85	0.511317 ± 12	−25.4	0.3	0.4	0.511214 ± 10	−25.1	0.3	42.8	0.282652 ± 16	−4.7	0.6	0.6	0.72
BIL06	260	52.99	−52.61	CTD	50	Surface	33.62	0.01	26.99	7.40	0.511426 ± 12	−23.3	0.3	0.4	0.511287 ± 8	−23.6	0.3	36.5	0.282729 ± 16	−2.0	0.6	0.6	0.80
HL08	3480	42.36	−61.35	CTD	2500	NEADW	34.93	2.96	27.83	5.98	0.511971 ± 4	−12.7	0.3	0.4				19.1	0.282776 ± 11	−0.3	0.4	0.6	0.84
HL11	4515	41.78	−60.91	CTD	3750	DSOW	34.89	1.99	27.89	6.03	0.511958 ± 6	−12.9	0.3	0.4				23.6	0.282609 ± 10	−6.2	0.3	0.6	1.03

All $^{143}Nd/^{144}Nd$ ratios were normalized to the accepted JNdi-1 standard value of 0.512115 (Tanaka et al., 2000). All $^{176}Hf/^{177}Hf$ ratios were normalized to the accepted JMC475 standard value of 0.28216 (Nowell et al., 1998).

Hafnium and neodymium isotopic compositions are expressed in epsilon units as deviations from the Chondritic Uniform Reservoir 0.512638 for Nd and 0.282785 for Hf (Jacobsen and Wasserburg, 1980; Bouvier et al., 2008; respectively).

1. *Indicates the samples that were measured at GEOMAR, Kiel, Germany.

Table 2
List of the abbreviations used in the text.

Abbreviation	Full name	Description
NADW	North Atlantic Deep Water	Represents the mixture of intermediate and deep waters formed within Arctic and subarctic
WGC	West Greenland Current	Flows northward along the coast carrying water from Denmark Strait
LC	Labrador Current	Fresh-water-laden current that flows south along the Labrador coast, formed due to admixture of outflows from Hudson Strait, Davis Strait and the waters of West Greenland Current
NAC	North Atlantic Current	Originates in the Gulf Stream, flows north along the east side of Grand Banks, where it turns east and flows across the ocean
IW/IC	Irminger Current or Irminger Water	Counterclockwise flow of warm and salty water around the rim of the Labrador Sea, which originates in the Irminger Sea
LSW	Labrador Sea Water	Formed due to the admixture of warmer saltier water of tropical origin (North Atlantic Current, Irminger Water) with polar outflows and admixtures from the shelf and upper slope (West Greenland Current and Labrador Current)
DWBC	Deep Western Boundary Current	Continuation of Deep North Boundary Current, formed due to admixture of Iceland Scotland Overflow Water and Denmark Strait Overflow Water, flowing southward to the Southern Ocean and incorporating the deep waters from the Labrador Sea
SLSW	Labrador Sea Water 2008	Formed after 1994, when the convection was weaker
DLSW	Labrador Sea Water 1987–1994	Remnants of the old Labrador Sea Water produced between 1987 and 1994
NEADW	North Eastern Atlantic Deep Water	Formed by the admixture of Iceland Scotland Overflow Water, modified North Atlantic Water, Labrador Sea Water and Eastern Lower Deep Water
ISOW	Iceland Scotland Overflow Water	Dense water overflow coming from Norwegian Seas through the Faroe Bank Channel, admixed with Modified North Atlantic Water and Labrador Sea Water
ISW	Iceland Slope Waters	Formed through a mixing of the original ISOW with Atlantic thermocline water near the Faroes. Flows along the slopes of Iceland and Reykjanes Ridge, until it enters Irminger Sea
MNAW	Modified North Atlantic Water	Originates from the North Atlantic Current
ELDW	Eastern Lower Deep Water	Derived from Antarctic Bottom Water and flows through the entire Atlantic Ocean until it enters the Subpolar North Atlantic region from the East within Deep Eastern Boundary Current off the European coast
DSOW	Denmark Strait Overflow Water	Enters the Labrador Sea at the base of the continental slope off Cape Farewell, Greenland as a part of Deep Western Boundary Current
SPMW	SubPolar Mode Waters	Formed due to mixing of the water masses in the Northern North Atlantic of subtropical and polar origin, occupies the upper 1000 m of the North Atlantic Subpolar Gyre

Water mass definitions are based on: Kearns and Rossby (1998), Lacan and Jeandel (2004a,b, 2005), Yashayaev and Clark (2006), Straneo and Saucier (2008).

teristics ($T \sim 2.96$ °C) similar to NEADW across the Labrador Sea, but a slightly higher salinity of 34.92 (Fig. 2B, D).

Denmark Strait Overflow Water (DSOW) is the densest water mass found in the Labrador Sea. It is noticeably colder, fresher and more oxygenated than NEADW (Yashayaev and Dickson, 2008). Its presence below NEADW is identified at stations 15.5 and 17.5 based on maximum oxygen concentrations ~6.7 ml/l at the bottom. These waters are denser than 27.9 kg/m^3, salinities range between 34.89 and 34.90 and the potential temperature is near 1.48 °C. The bottom sample at station 13.6 although falling within the same density and salinity range, has slightly higher potential temperature and lower oxygen concentration, suggesting that this sample does not represent pure DSOW. Similar characteristics are recorded along the Halifax line at st. HL11, where salinity is ~34.89 similar to an average value of 34.90 for DSOW along the AR7W transect (Fig. 2B) and temperature of ~1.99 °C, which is, however, warmer than in the Labrador Sea (1.48 °C).

The mixture of the deep water masses described above results in the formation of the core of NADW, which leaves the Labrador Sea in a southerly direction, ultimately occupying water depths between 1000 and 4000 meters (Schmitz, 1996).

2.3. Methods

Seawater samples were collected in 10 L Niskin bottles attached to a CTD rosette and directly filtered through Acropac 0.45 μm filter cartridges into 20 L pre-cleaned cubitainers. Subsequently, all samples were acidified with distilled concentrated HCl to pH ≈ 2. A one liter aliquot from every sample was kept separate in polyethylene bottles after acidification for precise Nd and Hf concentration measurements by isotope dilution (Stichel et al., 2012a). The remaining water was further processed in the clean laboratory following established methods (Rickli et al., 2009; Stichel et al., 2012a). The trace metals were preconcentrated by co-precipitation with a pre-cleaned Fe chloride solution. An ethyl ether step was applied to remove most of this iron in preparation for column chemistry. To separate Hf and Nd from the seawater matrix, three sets of ion exchange columns were used: cation columns with

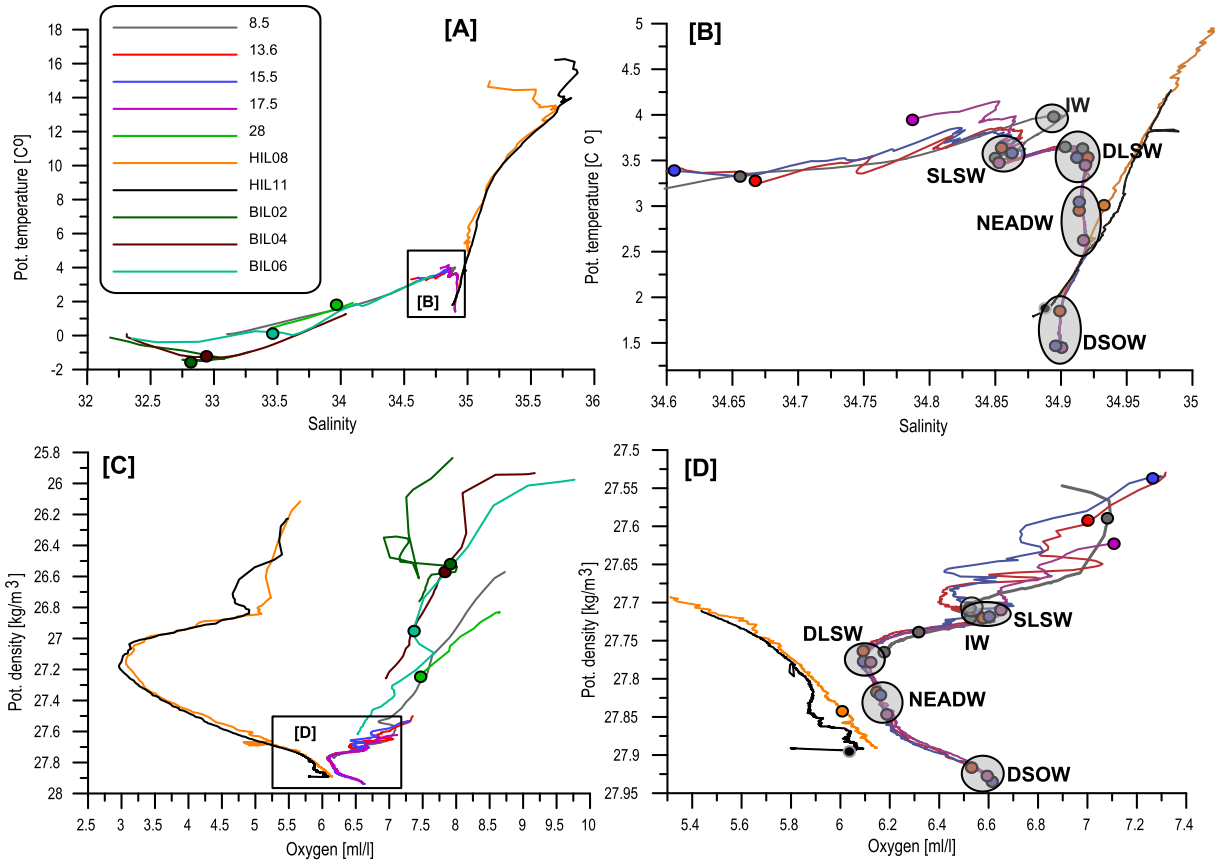

Fig. 2. CTD data for all stations. (A) Salinity vs. temperature. (B) Enlarged version of A for deep waters. (C) Density vs. oxygen concentration. (D) Enlarged version of C for deep waters. Light grey circles denote the major prevailing water masses.

AG 50W-X8 resin (200–400 dry mesh), columns loaded with Eichrom Ln-Spec resin with a bead size of 50–100 μm for Nd purification and a third set of columns loaded with Eichrom Ln-Spec resin with a bead size of 100–150 μm for Hf purification (Pin and Zalduegui, 1997; Münker et al., 2001).

Most Nd isotope measurements were carried out on a Thermo Finnigan Neptune Plus MC-ICP-MS at the Max Planck Research Group for Marine Isotope Geochemistry in Oldenburg, Germany. Only samples with Nd concentrations higher than 40 ng in the resulting 1 ml solution after purification were measured on the Nu Plasma MC-ICP-MS at GEOMAR. Neodymium isotopic compositions were corrected for instrumental mass bias to $^{146}Nd/^{144}Nd = 0.7219$ applying an exponential mass fractionation law. All $^{143}Nd/^{144}Nd$ ratios were normalized to the accepted JNdi-1 standard value of 0.512115 (Tanaka et al., 2000). The repeated measurement of one of the samples ($n = 3$) gave a 2 S.D. = 0.29. The external reproducibility on both instruments was between 0.3 and 0.4 (2 S.D.) based on repeated measurement of the JNdi-1 standard ($n = 23$) and an internal laboratory standard ($n = 10$) run at 30 ppb and 10 ppb at the GEOMAR and in Oldenburg, respectively. Internal measurement errors were smaller than the external errors for all samples with the exception of st. 17.5, 3000 m and st. 17.5, 80 m (0.5 εNd, 2 S.E.M.). The procedural blanks (for laboratory analysis) for Nd were below 2% of the sample Nd content (~300 pg) and are considered negligible. Replicates measured on both mass spectrometers gave the same results within analytical errors (Table 2).

Given that 20 L of water were available for Hf isotopic analysis, sample amounts corresponded to 1.6–4.3 ng of Hf only. Hafnium isotope compositions were measured on a Thermo Neptune Plus MC-ICP-MS at ETH Zurich yielding total Hf ion beams of $\geqslant 1.1$ V/ppb (10^{11} Ω resistor). Measured Hf isotope compositions were corrected for instrumental mass bias to $^{179}Hf/^{177}Hf$ of 0.7325 applying an exponential mass fractionation law. External reproducibility was estimated from repeated measurements of the JMC475 standard at a concentration of 5 ppb and corresponded to 0.6 εHf (2 S.D., $n = 12$, 20 and 22). Internal errors and beam sizes of the sample measurements were in most cases similar to the run standards (internal errors ranging between 0.4 and 0.6, 2 S.E.M.) indicating that the error estimate from standard measurements is applicable for most samples (Table 1). Procedural blanks were less than 3% of the sample Hf contents (less than 28 pg) and are considered negligible.

Isotope dilution measurements of Hf and Nd concentrations were carried out on the Nu Plasma MC-ICP-MS at GEOMAR. Hafnium and Nd spike solutions, enriched in

^{178}Hf, ^{149}Sm and ^{150}Nd, were added to every sample gravimetrically. Neodymium and Hf preconcentration based on iron co-precipitation was applied and purification was achieved by a single step column separation (AG50W-X8, 200–400 dry mesh). A detailed description of the method and uncertainties is presented in Stichel et al. (2012a).

Rare earth element (REE) concentrations were measured on an 8 ml sample loop using an online preconcentration technique (OP) ICP-MS at GEOMAR employing an automated "SeaFast" system (Elemental Scientific Inc.) coupled to an Agilent 7500ce ICP-MS (Hathorne et al., 2012). During the measurements, reference seawater from the Bermuda Atlantic Time Series (BATS, 15 m; BATS, 2000 m, van de Flierdt et al., 2012) was used to track the reproducibility and accuracy of the data (Table 3). "Empty seawater", from which all the REEs had been removed by Fe-coprecipitation, was used as a procedural blank, which was subtracted from the data.

Neodymium concentrations were measured by OP-ICP-MS as well as by isotope dilution. The paired *t*-test for dependent variables showed no significant difference between these two methods ($t(25) = 4.76$, $p = 0.0001$), as has been demonstrated previously (Hathorne et al., 2012). Further discussion of Nd concentrations in the context of Nd isotopes will utilize the more precise isotope dilution data.

3. RESULTS

3.1. REE and Hf concentrations in seawater

The REE concentrations (OP-ICP-MS) in the surface waters of the Labrador Sea along the AR7W transect exhibit little variability but are slightly enriched in the light REEs (La–Nd) compared to the deeper waters (Fig. 3). Below the surface, rare earth element concentrations are invariable with depth with only two exceptions (Fig. 3). A marked increase in Gd concentration from 4.76 pmol/kg to 19.81 pmol/kg is observed in the deepest sample of st. 15.5 coincident with an increase of Yb from 5.16 pmol/kg up to 6.61 pmol/kg. Neodymium concentrations (ID) (Fig. 4A) in surface waters across the Labrador Sea (AR7W transect, Fig. 1) range from 19.2 pmol/kg at st. 15.5 to 20.2 pmol/kg at st. 8.5. Hafnium concentrations vary between 0.62 pmol/kg at st. 17.5 and 1.02 pmol/kg at st. 15.5 and st. 13.6 (Fig. 4B). Station 13.6 in general shows higher LREE concentration than other stations along the transect at corresponding depths.

The surface water samples along the Belle Isle line from 50 m depth collected north of Newfoundland (BIL02; BIL04; BIL06) have light and middle REE concentrations up to an order of magnitude higher than the surface waters across the Labrador Sea (AR7W transect, Fig. 3). Neodymium concentrations are about twice as high as in the open Labrador Sea ranging from 36 to 48 pmol/kg, whereas Hf concentrations are not elevated and range from 0.72 to 1.13 pmol/kg. At these stations, the Nd concentrations systematically decrease with distance from the shore (Fig. 4A) but no such trend is observed for the Hf concentrations (Fig. 4B). The surface sample collected in close proximity of the southern tip of Greenland (st. 28) exhibits lower REE concentrations than the surface samples collected north of Newfoundland, but still 10–60% higher than those collected along the AR7W transect for some of the REEs. Hafnium concentrations are similar in all surface samples. The deep water sample collected from the Halifax line off the coast of Nova Scotia (HL08, 2500 m) has REE and Nd (19.06 pmol/kg) concentrations similar to the corresponding depths along the AR7W transect. However, st. HL11, 3750 m has higher REE and Nd (23.63 pmol/kg) concentrations than observed at similar depths along the AR7W transect. Hafnium concentrations are similar to those along the transect at both stations.

3.2. Nd isotope compositions

The Nd isotope compositions of the four water depth profiles along the AR7W line (Fig. 4C) range from −16.8 (st. 15.5, 80 m) to −11 (st. 15.5, 3512 m). The εNd signatures at stations 13.6 and 15.5 become continuously more radiogenic with depth. At station 17.5, two samples collected from the upper 2000 m of the water column yield an average εNd signature of ∼−14 being identical within analytical uncertainty. Below a depth of 2000 m, the εNd signature becomes more radiogenic, reaching −11.6 near the bottom at 3670 m. The most radiogenic εNd value of −11 is observed in the lowermost sample of station 15.5, 3512 m. At the shallower station 8.5 (water depth of 1702 m), the εNd signature of the profile shows uniform values throughout the water column (average $\varepsilon Nd = -13.9$) with the exception of the less radiogenic surface sample ($\varepsilon Nd = -15.8$). The two deep water samples collected along the Halifax line (HL11, 3750 m and HL08, 2500 m) show virtually identical εNd signature with an average of −12.8. These results are consistent with previous εNd observations at neighboring sites in the Labrador Sea (Hudson 83-036, station 9, 2550 m and station 11, 2500-–850 m) (Piepgras and Wasserburg, 1987).

Near surface waters along the AR7W transect have less radiogenic values than the deep samples, ranging between −16.8 (st. 15.5, 80 m) and −14.9 (st. 17.5, 80 m). A similarly low Nd isotope composition is also observed at shallow depth close to the southern tip of Greenland (st. 28, 100 m, $\varepsilon Nd = -15.7$). Surface samples collected along the Belle Isle line show the most unradiogenic values of this study ranging from −25.4 (st. BIL02, st. BIL04, both 50 m) to −23.3 (st. BIL06, 50 m), clearly documenting terrestrial input from the Precambrian terrains of the Canadian Shield. With distance from shore the εNd signature becomes slightly more radiogenic.

3.3. Hf isotope compositions

Hafnium isotope signatures range from +0.3 (st. 17.5, 3000 m) to −11.7 (st. 28, 100 m), which is the least radiogenic εHf value for seawater measured globally so far (Fig. 4D). Surface samples along the Belle Isle line off Newfoundland range from −9.2 at BIL02 to −2 at BIL06, with εHf signatures becoming systematically more radiogenic with distance from the coast. Surface seawater signatures

Table 3
REE concentrations obtained by OP ICP-MS (pmol/kg) and Nd concentrations obtained via the isotope dilution method (pmol/kg). La/Yb ratio and Ce anomaly are also shown. Additionally, GEOTRACES BATS intercalibration results are included (van de Flierdt et al., 2012).

Station	Depth [m]	La [pmol/kg]	Ce [pmol/kg]	Pr [pmol/kg]	Nd [pmol/kg]	Nd (ID) [pmol/kg]	Sm [pmol/kg]	Eu [pmol/kg]	Gd [pmol/kg]	Tb [pmol/kg]	Dy [pmol/kg]	Ho [pmol/kg]	Er [pmol/kg]	Tm [pmol/kg]	Yb [pmol/kg]	Lu [pmol/kg]	La/Yb[a]	Ce/Ce*[b]
8.5	150	29.7	11.3	5.42	22.7	20.2	4.17	0.96	5.90	0.85	6.04	1.64	5.11	0.72	4.96	0.83	0.35	0.20
8.5	400	26.3	6.44	4.53	18.4	18.0	3.79	0.92	4.71	0.84	5.82	1.53	4.92	0.82	4.78	0.81	0.33	0.13
8.5	750	27.7	6.91	4.40	19.9	18.6	3.71	0.77	4.92	0.84	6.01	1.59	5.52	0.77	4.41	0.80	0.37	0.14
8.5	1050	27.3	6.61	4.72	21.3	18.0	3.20	0.91	4.99	0.78	6.20	1.54	5.17	0.76	4.99	0.78	0.32	0.13
8.5	1500	25.7	5.28	4.35	19.2	18.0	3.56	0.91	4.28	0.77	5.74	1.60	5.23	0.77	4.81	0.82	0.32	0.11
13.6	100	32.8	12.6	5.69	23.0	19.6	4.00	0.95	5.71	0.88	6.20	1.64	5.69	0.84	4.74	0.89	0.41	0.21
13.6	1000	27.1	6.76	4.51	19.7	18.4	3.16	0.84	4.77	0.81	5.77	1.53	4.95	0.75	4.58	0.74	0.35	0.14
13.6	1700	26.6	6.21	4.64	18.4	18.0	3.88	0.88	5.21	0.76	6.11	1.60	5.48	0.84	4.75	0.80	0.33	0.13
13.6	2400	24.4	5.47	4.27	16.9	16.7	3.97	0.92	5.19	0.79	5.85	1.62	5.01	0.75	4.71	0.85	0.31	0.12
13.6	3360	26.2	7.22	4.63	20.0	18.5	4.01	0.89	5.89	0.84	5.76	1.58	5.09	0.77	4.81	0.81	0.32	0.15
15.5	80	29.5	10.8	5.12	20.9	19.2	3.78	0.88	4.77	0.73	5.55	1.42	4.94	0.75	4.31	0.70	0.41	0.20
15.5	1000	26.5	6.20	4.41	18.4	18.5	3.11	0.86	4.88	0.84	5.86	1.49	5.00	0.80	4.56	0.77	0.34	0.13
15.5	1700	24.6	4.79	4.30	18.6	19.3	3.49	0.81	4.74	0.75	5.99	1.72	5.24	0.83	4.82	0.80	0.30	0.11
15.5	2300	24.8	6.10	4.43	18.8	16.6	3.96	0.94	4.76	0.86	5.98	1.47	5.46	0.77	5.16	0.82	0.28	0.13
15.5	3512	26.3	6.50	4.43	19.4	18.1	3.97	1.04	$19.8	0.74	6.55	1.65	5.30	0.79	6.61	0.86	0.24	0.14
17.5	80	26.7	10.6	4.76	19.5	19.7	3.36	0.82	4.48	0.81	5.87	1.51	4.71	0.75	4.34	0.77	0.36	0.21
17.5	1000	28.0	7.58	4.94	20.2	18.6	3.54	0.81	5.11	0.90	5.95	1.62	5.34	0.69	4.87	0.78	0.34	0.15
17.5	2000	27.2	8.45	4.49	19.1	19.7	3.52	0.78	5.04	0.80	5.94	1.62	5.30	0.75	5.00	0.82	0.32	0.17
17.5	3000	23.5	5.36	3.85	16.4	15.2	3.07	0.78	3.98	0.72	5.81	1.41	4.69	0.67	4.51	0.76	0.31	0.13
17.5	3670	25.2	6.22	3.98	17.4	16.8	3.16	0.72	4.92	0.78	5.01	1.56	4.70	0.69	4.75	0.78	0.31	0.14
28	100	36.3	18.6	6.23	24.9	26.0	5.00	1.21	6.21	0.97	6.80	1.65	6.01	0.87	5.17	0.86	0.42	0.28
BIL02	50	82.9	40.0	12.8	52.6	48.2	7.08	1.64	8.70	1.35	9.12	2.25	6.84	1.03	6.52	1.13	0.75	0.26
BIL04	50	77.1	35.1	11.5	44.9	42.8	6.95	1.41	8.58	1.21	7.86	1.99	6.79	1.01	6.25	0.91	0.73	0.27
BIL06	50	63.3	28.2	10.1	40.6	36.5	6.65	1.34	7.68	1.19	8.59	2.12	6.26	0.92	6.36	1.12	0.59	0.25
HL08	2500	26.9	6.89	4.64	20.1	19.1	3.83	0.99	4.84	0.88	5.96	1.64	5.19	0.78	4.81	0.83	0.33	0.14
HL11	3750	34.5	9.58	5.93	25.1	23.6	5.23	1.16	6.04	0.95	6.44	1.77	5.82	0.83	5.61	0.87	0.36	0.15
2S.D.*[e]		0.76	0.56	0.25	0.73		0.38	0.06	0.5	0.12	0.43	0.14	0.34	0.09	0.38	0.08		
GEOTRACES BATS intercalibration																		
BATS 15 m																		
Average $n = 7$		14.9	10.8	3.2	15.1		3.29	0.79	4.72	0.82	5.98	1.56	4.99	0.68	4.10	0.67		
2σ		0.76	0.56	0.25	0.73		0.38	0.06	0.50	0.12	0.43	0.14	0.34	0.09	0.38	0.08		
BATS 2000 m																		
Average $n = 3$		24.1	4.16	4.1	18.0		3.09	0.87	4.79	0.79	5.72	1.54	5.10	0.76	4.75	0.84		
2σ		0.41	0.08	0.17	1.34		0.89	0.08	0.53	0.07	0.29	0.09	0.43	0.08	0.24	0.03		
[c]BATS 15 m																		
Average $n = 17$		14.7	12.0	3.12	14.1		3.21	0.89	4.83	0.79	5.90	1.49	4.80	0.70	4.16	0.67		
2σ		2.21	2.74	0.37	1.24		0.36	0.11	0.55	0.08	0.52	0.13	0.42	0.07	0.51	0.09		
[d]BATS 2000 m																		
Average $n = 17$		23.6	5.12	4.03	17.3		3.45	0.91	4.84	0.79	5.80	1.52	5.04	0.74	4.76	0.81		
2σ		2.79	2.27	0.35	1.22		0.34	0.10	0.53	0.08	0.38	0.09	0.25	0.05	0.25	0.04		

[a] $Ce/Ce^* = Ce/((La + Pr)/2)$, values used are normalized to PAAS.
[b] La/Yb = La/Yb, values used are normalized to PAAS.
[c] Uncertainties and average values from the study by van de Flierdt et al. (2012) for BATS 15 m.
[d] Uncertainties and average values from the study by van de Flierdt et al. (2012) for BATS 2000 m.
[e] Uncertainties of the REE measurement by OP-ICP MS based on the repeated measurement of BATS 15 m, $n = 7$ (van de Flierdt et al., 2012).

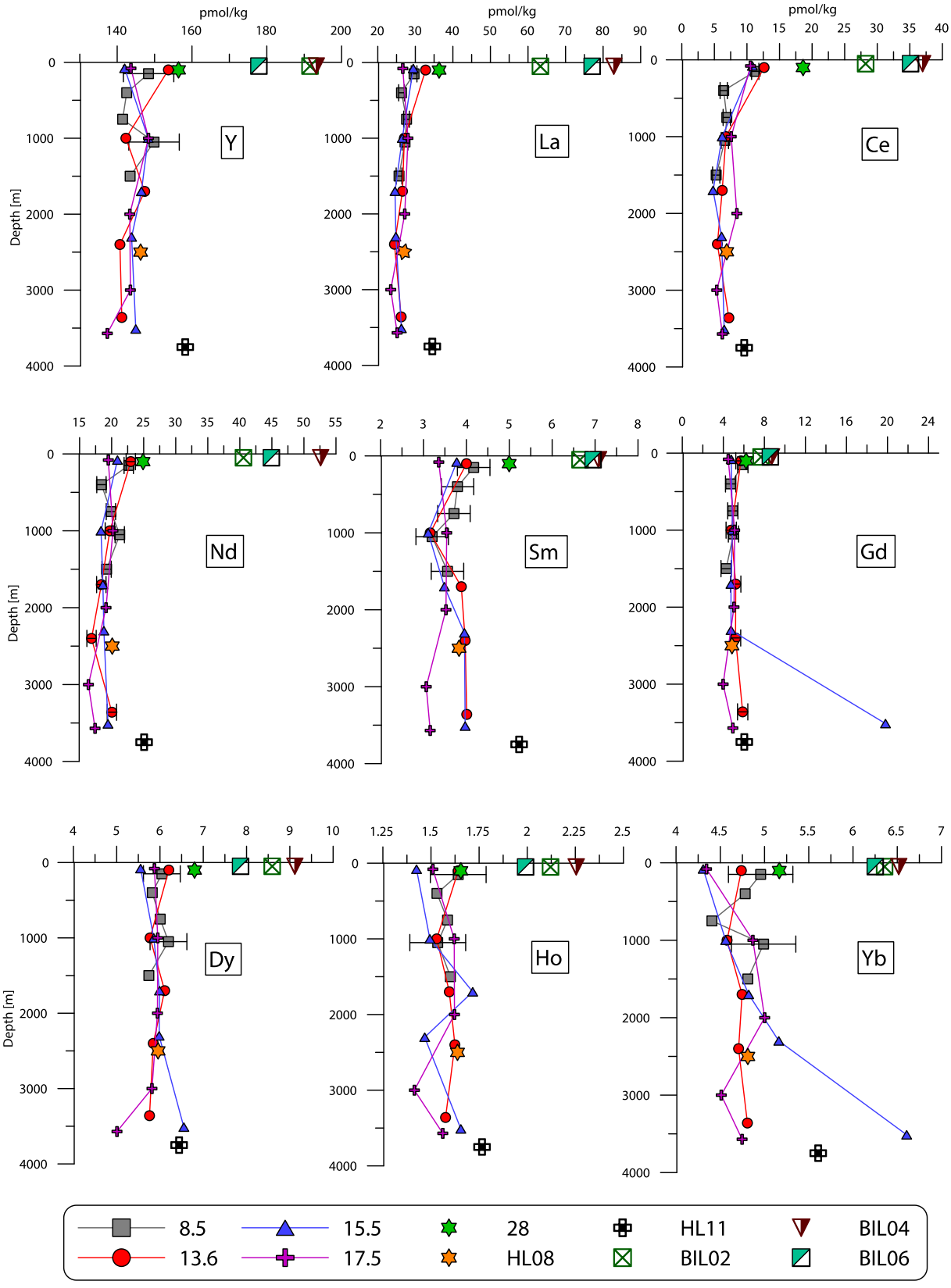

Fig. 3. Concentrations of individual rare earth elements versus water depth based on OP-ICP-MS analysis. The error bars shown on the plots for one profile denote the 2S.D. reproducibility of all data.

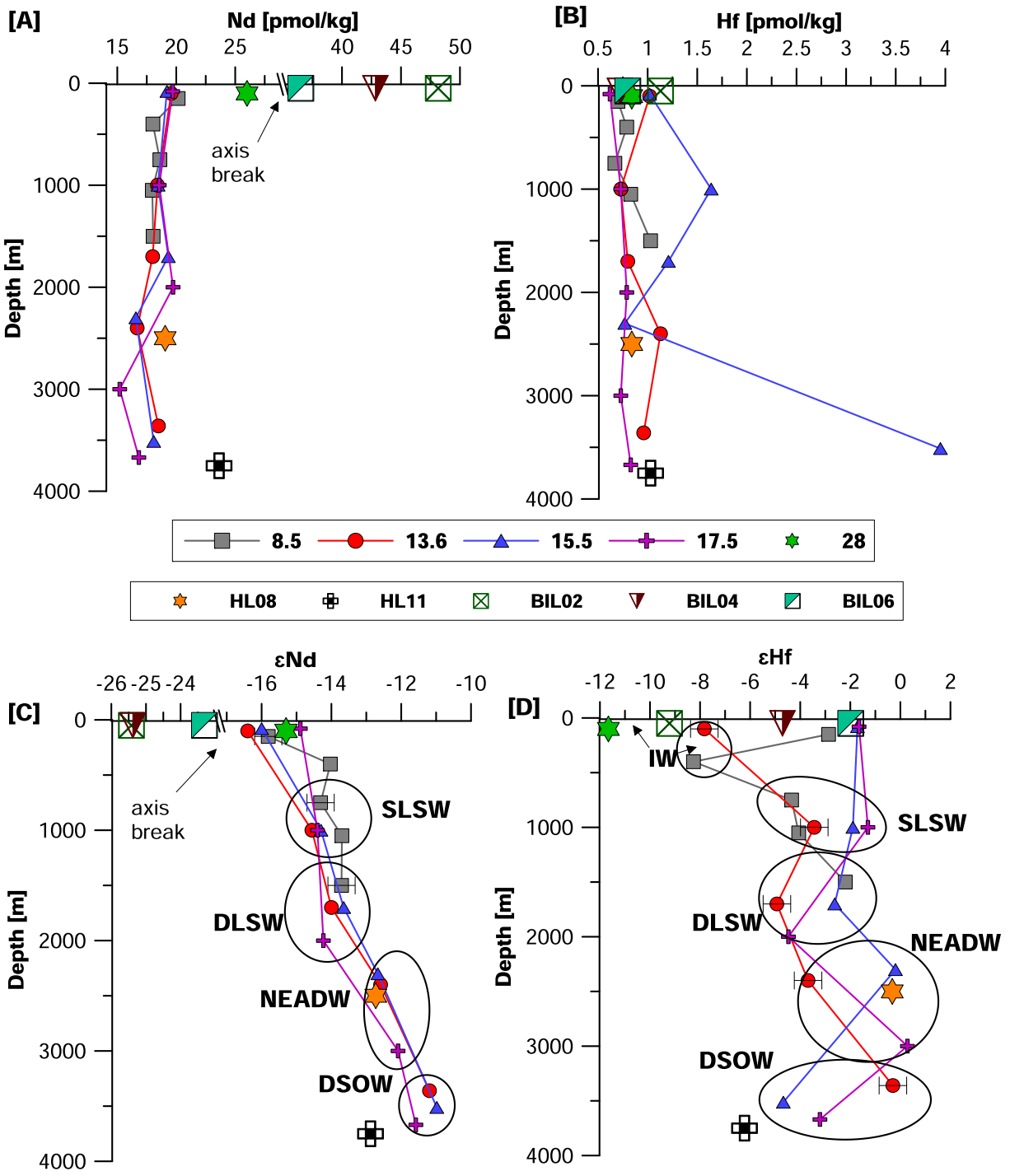

Fig. 4. Depth distributions of εHf and εNd signatures and Hf and Nd concentrations (isotope dilution method). (A) Nd concentrations in pmol/kg. (B) Hf concentrations in pmol/kg. (C) εNd signature. (D) εHf signature. Black circles denote samples representing the same water masses.

from the four water depth profiles are generally invariant (average εHf = −2) with the exception of the sample at st. 13.6 (100 m, εHf = −7.8).

Unlike εNd, the εHf signatures of the four water depth profiles along the AR7W transect show a high degree of variability in the water column, with stations 15.5 and 17.5 showing similar distributions. Two samples from the upper 1000 meters yield an average εHf signature of −1.7 (Fig. 4D, Table 2) whereas below the εHf signature is less radiogenic at depths of 1700–2000 m and more radiogenic again between 2300 and 3000 m. At the bottom the signature changes to less radiogenic values again, which includes

the sample with the anomalously high Gd and Yb concentrations of st. 15.5. The Hf isotope composition at st. 8.5 is most radiogenic near the bottom at 1500 m ($\varepsilon Hf = -2.2$) and shows a distinct unradiogenic peak below the surface at 400 m ($\varepsilon Hf = -8.3$). At st. 13.6 the εHf signature becomes more radiogenic with depth below 1700 m.

The deep sample collected along the Halifax line at st. HL08, 2500 m has an εHf signature of −0.3, which is similar to the observation at st.15.5, 2300 m ($\varepsilon Hf = -0.2$) and st. 17.5, 3000 m ($\varepsilon Hf = +0.3$). The sample from st. HL11, 3750 m, in contrast, shows a highly unradiogenic εHf signature of −6.2, which is about 2 εHf units less radiogenic, than at the corresponding depth along the AR7W transect (st. 17.5, 3670 m $\varepsilon Hf \sim -3.2$ and st. 15.5, 3512 m $\varepsilon Hf \sim -4.7$).

4. DISCUSSION

4.1. REE distribution and patterns and Hf concentration

The lack of variability in most of the REE and Hf concentrations with water depth in the Labrador Sea (AR7W transect), and essentially identical REE patterns normalized to Post-Archean Average Australian Sedimentary Rock (PAAS; McLennan, 2001) for different water masses (Figs. 3 and 5) suggest efficient vertical mixing in the region. However, at the same time we observe variability in εHf and a systematic gradual change in εNd towards more radiogenic signatures with water depth (Fig. 4). These opposing observations can be reconciled if waters advected into the Labrador Sea are characterized by minor differences in their REE, Hf, and Nd concentrations. Previously published studies by Lacan and Jeandel (2004a,b, 2005) and Lambelet et al. (2015) show that rare earth element patterns and concentrations delivered to the Labrador Sea through the Denmark Strait via ISOW and IW are essentially uniform. Unfortunately, no Hf concentration data are available to infer similar preformed concentrations for Hf. Another potential source with distinct REE signature are Baffin Bay waters and waters from the Hudson Strait, which are highly enriched in Nd and REE (Stordal and Wasserburg, 1986; Goldstein and Jacobsen, 1988). Admixture of these waters into the Labrador Sea should result in variations of REE concentrations but these waters are not dense enough to directly contribute to the deep water mass formation in the region, which restricts their influence to the LC flowing at the surface along the coast (Lacan and Jeandel, 2005). This could explain why some of the REE concentrations (La, Ce, Nd, Sm, Gd, Ho and Dy) at stations 13.6 and 8.5 in general are slightly higher in surface waters than at corresponding depths of two other stations (Fig. 3). This suggests that the uniform signal supplied to the Labrador Sea together with restricted influence of the coastal waters are responsible for the homogenous distribution of the REEs throughout the water column rather than intensive vertical mixing occurring in other oceanographic regions (Sholkovitz and Schneider, 1991; Nozaki and Alibo, 2003; Hathorne et al., 2015).

The small changes in Hf concentrations between some of the stations at a given depth appear to be unsystematic. Although vertical Hf concentration profiles are flat, spatial variability in Hf concentrations at different stations within the same water masses may be explained by a combination of factors such as Hf being influenced to a large extent by local terrestrial inputs and the difference in time it takes DSOW and NEADW within the Labrador Sea to record

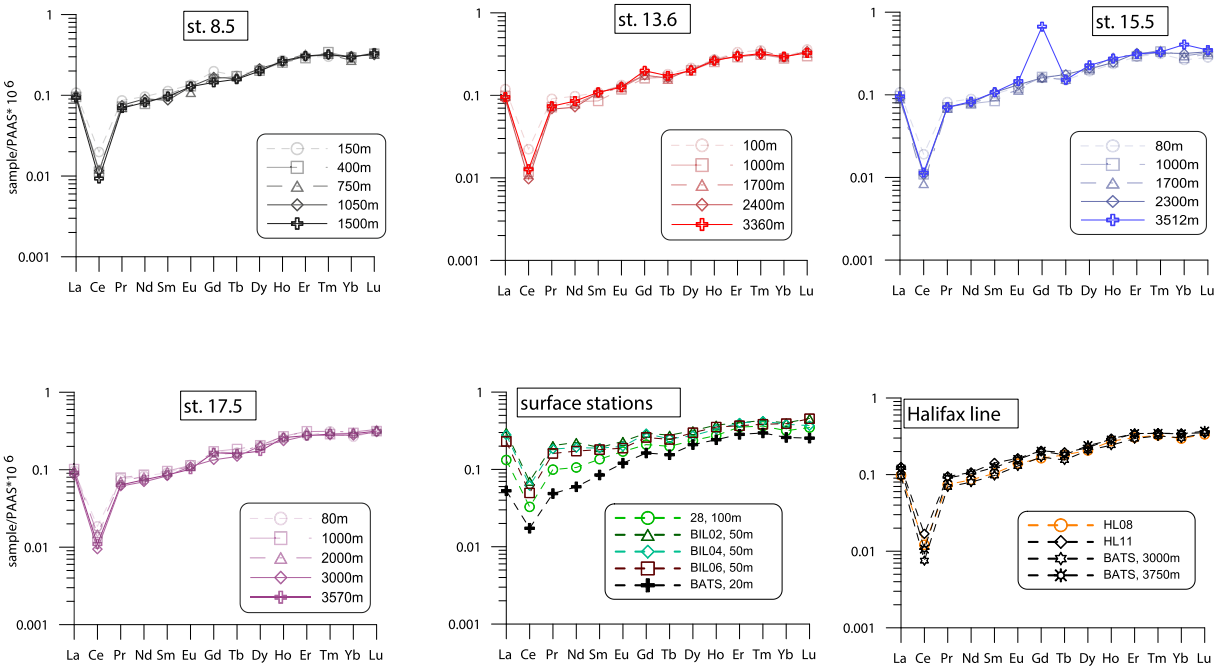

Fig. 5. Rare earth element patterns normalized to Post-Archean Australian Sedimentary rocks (PAAS) (McLennan, 2001), additionally BATS 20 m, BATS 3000 m and BATS 3750 m normalized to PAAS are shown for comparison (Pahnke et al., 2012).

the change in LSW formation (Yashayaev et al., 2008, more details in Section 4.2). This would result in different Hf concentrations, as the waters move around the Labrador Sea, reflecting the signal of temporally changing inputs. In addition, the differences in Nd concentrations in comparison to data from Lacan and Jeandel (2005) at neighboring sites from July 1999 suggest annual or seasonal variability. The intermediate waters (~1600 m) sampled in 2013 have 1 pmol/kg higher Nd concentrations than the waters sampled from corresponding depths in 1999 while deep waters (>2500 m) sampled in 2013 have lower (3–5 pmol/kg) Nd concentrations than waters sampled in 1999. This may be caused by the annual variability in LSW production. However, samples of deep waters in the study by Lacan and Jeandel (2005) were not filtered, which also could have resulted in higher Nd concentrations. One surface sample of their study which was filtered, showed results identical to the unfiltered concentrations, which is, however, not sufficient to establish whether or not the filtration has a significant effect on Nd concentrations, especially for deep waters. Concentrations of both elements, therefore, could depend on the intensity of the winter convection, which, however, would need to be confirmed by repeated measurements of Hf and Nd at the same stations. The local maximum in Hf concentration observed at st. 15.5, 3512 m most likely originates from partial dissolution of suspended sediment in an extended nepheloid layer.

Comparison of the coastal samples collected from both sides of the Labrador Sea, shows a clear distinction in signal of the terrestrial inputs coming from Canada and Greenland. Samples collected from stations BIL02, BIL04, and BIL06 along the Belle Isle line have elevated REE concentrations with a distinct LREE enrichment compared to station 28. This enrichment can still be clearly seen in the REE patterns normalized to 15 m depth Bermuda Atlantic Time series waters (BATS, Fig. 6), which represent the waters coming from the south, indicating that Canadian terrains are a major contributor of REEs to the surface waters of the Labrador Sea. Although the fresh waters supplied to these sites are not dense enough to be vertically mixed within the Labrador Sea, which is similar to observations in the Arctic Ocean (Porcelli et al., 2009), the LREE signal appears to be transported into deeper waters as it is observed in the NADW (Fig. 6, Halifax Line, this study, and BATS 3000 m and 3750 m, Pahnke et al., 2012). This may be explained by release of REE's from the dissolution of suspended particles (Rousseau et al., 2015) transported from the Hudson Bay estuary within the surface waters of the LC.

4.2. Isotopic signature of different water masses

4.2.1. DSOW

Denmark Strait Overflow Water is the densest water mass in the Labrador Sea with potential densities above 27.90 kg/m^3, which corresponds to the bottom samples collected from stations 17.5, 3670 m, 15.5, 3512 m and 13.6, 3360 m. These waters have a uniform εNd signature of ~ −11.3 and a broader range of εHf between −0.3 (st. 13.6, 3360 m) and -4.7 (st. 15.5, 3512 m). The most radiogenic εHf value of −0.3 could be explained by the admixture of overlying NEADW, which has a more radiogenic εHf signature (Figs. 4D, 7). This is supported by a higher temperature (+0.3 °C) and lower oxygen content (−0.2 ml/l, Fig. 2) recorded for this sample.

The εNd signature of DSOW between −11 and −11.6 is in a good agreement with previously published data from nearby locations (Lacan and Jeandel, 2005; Lambelet et al., 2015). The acquired εNd signature is also consistent with the mixing of the source waters contributing to DSOW in the Labrador Sea (Schmitz, 1996), a significant fraction of which is NEADW (εNd ~ −12.5) integrating contributions from unradiogenic LSW (εNd ~ −14.1) and Subpolar Mode Waters (SPMW) (on average −13 to −14) and mixing with the more radiogenic original DSOW before its entrainment into the Labrador Sea (−10 to −7) (Lacan and Jeandel, 2005). The Nd isotope signatures, however, only show subtle differences between DSOW and NEADW at any of the stations below 3000 m (Figs. 4D, 7). This is explained by the lack of significant differences in the source waters forming these water masses, which would also imply similar signatures for εHf. Although the overall εHf ranges of DSOW and NEADW largely overlap, the εHf values within each station exhibit a clear distinction between DSOW and NEADW of up to 4 εHf units. Less radiogenic values of DSOW might reflect the influence of highly unradiogenic IW, the signal of which was recorded at st. 28, 100 m (εHf = −11.7). An influence of highly unradiogenic terrestrial inputs from Greenland into DSOW is also possible. This is supported by higher Nd (>2 pmol/kg) and Hf (>0.2 pmol/kg) concentrations of the bottom samples at stations 13.6 and 15.5 than at st. 17.5, 3670 m, and higher Nd and Hf concentrations at st. 13.6, 3360 m than in average NEADW accompanied by higher concentrations of some light and middle REEs including La, Ce, Pr and Gd (Fig. 3). In addition, there is an εHf shift to less radiogenic values at st. 13.6, 1700 m (εHf = −4.9) and 13.6, 2400 m (εHf = −3.7) compared to the corresponding depths at stations 17.5 (εHf = −1.3, 1700 m) and 15.5 (εHf = −2.6 and −0.2, respectively).

The higher variability in εHf than in εNd may reflect the differences in the timing of DSOW and NEADW production and advection, which results in a higher sensitivity of DSOW to decadal changes. DSOW requires about 1 year to travel to the Labrador Sea, while NEADW only reaches the Labrador basin 5–8 years after formation (Yashayaev and Clark, 2006; Yashayaev et al., 2008). The εHf signature may then reflect decadal changes in local weathering inputs and distinct Hf isotope signatures of rocks along the different flow paths of DSOW and NEADW. To preserve such variability, the Hf residence time needs to be on the order of the mixing time of the water masses in the Labrador Sea. The almost complete absence of information on Hf fluxes from shelves and rivers limits our ability to quantitatively constrain the seawater residence time of Hf. The more homogeneous Hf signal outside of the Labrador Sea most likely reflects the remoteness from the marginal input fluxes along the water mass pathways. An overall shorter residence time of Hf than that of Nd likely results from the different chemical speci-

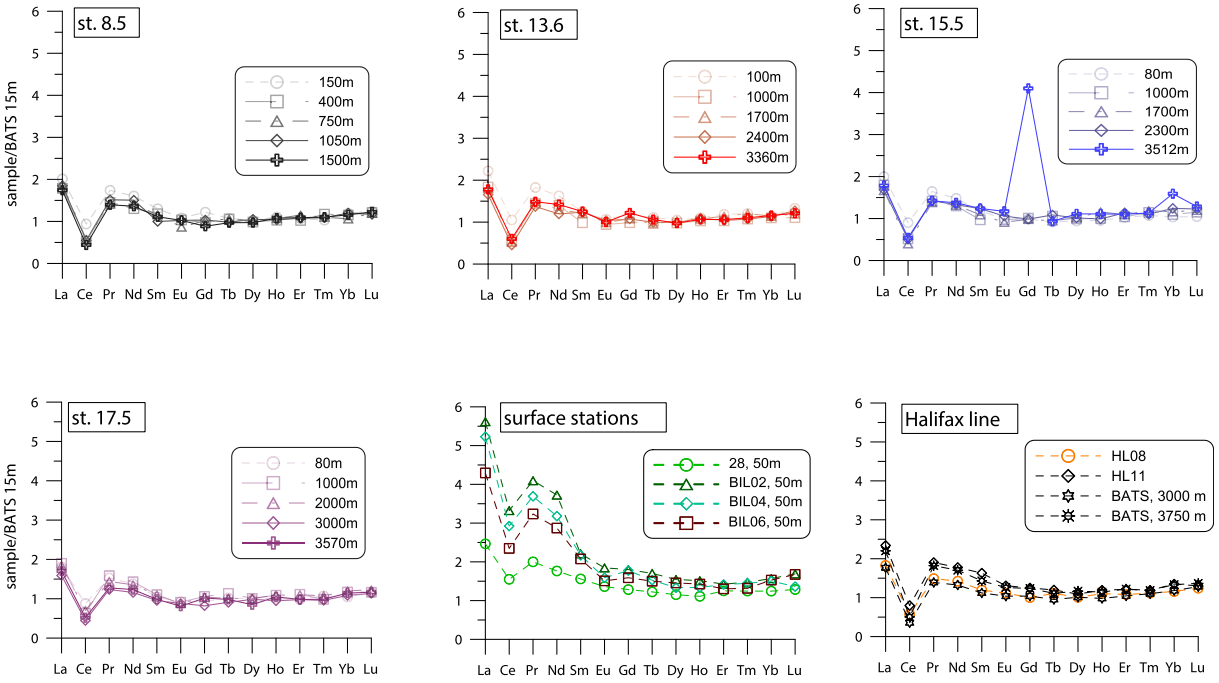

Fig. 6. Rare earth element patterns normalized to Bermuda Atlantic Time Series data values from 15 m from van de Flierdt et al. (2012).

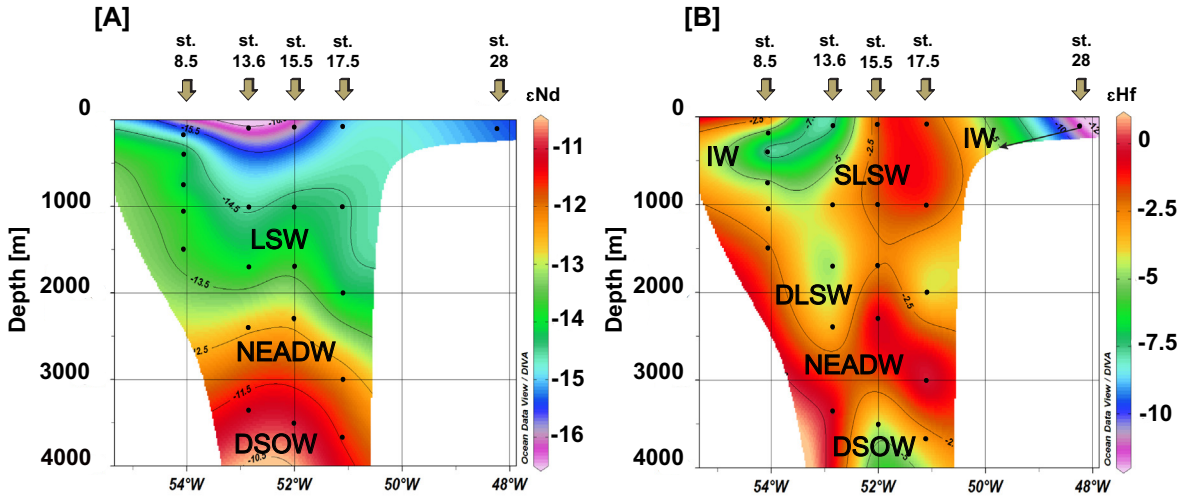

Fig. 7. Water mass distribution versus depth in the Labrador Sea based on their εNd (A) and εHf (B) signatures. Figure was created with ODV software (Schlitzer, 2015).

ations of these elements in seawater where Nd is dominated by carbonate complexes and Hf is mainly present as a hydroxide (Bruland, 1983). Variable Hf isotope compositions in the Labrador Sea are thus a function of the short residence times of the water masses and the degree of incongruent weathering inputs from the surrounding landmasses and their distinct εHf signatures, which can also explain the relatively high variability in Hf concentrations across the Labrador Sea.

The two deep samples from the Halifax line off the coast of Nova Scotia show a similar εNd signature near −12.8. In contrast, εHf differs by almost 6 units (st. HL11, 3750 m, −6.2 and st. HL08, 2500 m, −0.3). At station HL08, 2500 m, the εHf and εNd signatures are consistent with a NEADW origin, which is also indicated in hydrographic properties (Fig. 2). Station HL11, 3750 m, however, received significant contributions from a source other than DSOW, given that both εHf and εNd are significantly less radiogenic than DSOW (εNd ~ −11.3, εHf between −0.3 and −4.7) along the AR7W transect in the Labrador Sea. The hydrographic data indicate that these waters are less dense (<27.9 kg/m^3) and depleted in oxygen in comparison to DSOW. These waters are thus similar in hydrographic characteristics to st. 13.6, 3360 m but slightly warmer by

0.26 °C and slightly less saline by 0.01. This may indicate that this sample represents the advection of a mixture of upper NEADW with DSOW below. However, the signal recorded at st. HL11, 3750 m is still too unradiogenic in Hf in comparison to DSOW in the Labrador Sea. Unfortunately, the absence of Hf and Nd isotope data from the full water depth profiles along the Halifax line does not allow an unambiguous identification of the source of this shift and we can thus only speculate on its origin. One possible explanation is the intrusion of particle-loaded waters coming from land through the Gulf of Maine carrying highly unradiogenic values for both Nd and Hf isotopes as indicated by stations BIL02, BIL04, and BIL06 along the Belle Isle line (εNd between −25.9 to −23.3, εHf between −11.7 to −4.7) (Fig. 4C, D).

The other more likely explanation of the less radiogenic εHf signature at st. HL11 is exchange with resuspended sediments moving down the slope. This has previously been documented to be the cause for shifts in εNd without changing concentrations (“boundary exchange”) (Lacan and Jeandel, 2005; Wilson et al., 2012) and has also been suggested to influence the Hf isotope composition of seawater (Rickli et al., 2009; Zimmermann et al., 2009a). The movement of the resuspended sediment load down the slope may cause release and exchange with the particles through desorption/adsorption or partial dissolution of the particles. Additionally, assuming that the suspended loads mainly consist of sediments derived from the Precambrian Canadian terrain, one would expect highly unradiogenic Hf and Nd values. The shift in εHf and to a lesser extent of εNd to less radiogenic values than of DSOW recorded in the Labrador Sea, which is accompanied by elevated REE, Nd and Hf concentrations along the Halifax line at st. HL11, 3750 m in comparison to DSOW in the Labrador Sea, suggests dissolution and terrestrial input rather than any kind of “boundary exchange” process, which is also supported by the fact that this sample plots close to the zircon free sediment bearing array in εHf–εNd space, suggesting a more congruent weathering signal (Fig. 8).

4.2.2. NEADW

North Eastern Atlantic Deep Water was encountered at three stations between densities of 27.80–27.88 kg/m^3. The new Nd isotope data are consistent with previously published values (Lacan and Jeandel, 2005; Lambelet et al., 2015). The εNd signature of NEADW is in the range between −12.1 and −12.7. The εHf signature of NEADW ranges between −0.2 to +0.3. However, the sample collected within the NEADW density range from st. 13.6 at 2400 m shows a less radiogenic signature of −3.7, which is most likely explained by admixture of water from the upper layer of DLSW, which is not reflected, however, in hydrographic data. The more radiogenic εHf signature of NEADW in comparison to DSOW may reflect weathering of Icelandic basalts and dissolution of volcanic glasses, which are highly radiogenic and easily leachable (Pearce et al., 2013). Also, these waters have potentially spent more time in contact with basaltic rocks, due to longer travelling time of NEADW into the Labrador Sea (Yashayaev and Clark, 2006; Yashayaev et al., 2008), while DSOW is more likely to be under the influence of terrestrial inputs coming from Greenland.

The advection of NEADW outside of the Labrador Sea is traceable at st. HL08, 2500 m, where Hf (−0.3) and Nd (−12.7) isotope signatures are consistent with the average NEADW values. Salinity, temperature and density profiles clearly document NEADW presence, although with slightly lower oxygen concentrations (~0.2 ml/l) (Fig. 2).

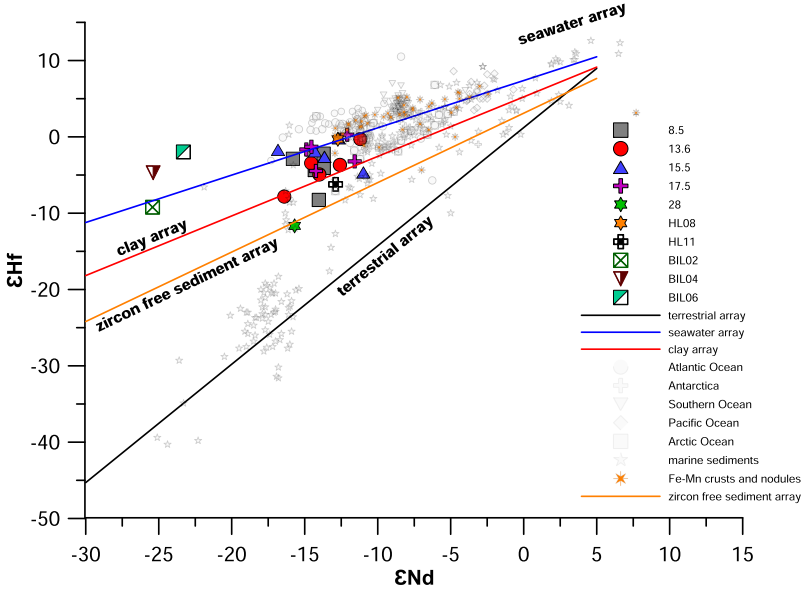

Fig. 8. εHf versus εNd of the seawater data of this study together with terrestrial array (Vervoort et al., 2011), seawater array (David et al., 2001), clay array (Bayon et al., 2016), and zircon free sediment array (Bayon et al., 2009). Data for seawater samples are compiled from Godfrey et al. (2009), Rickli et al. (2009, 2010, 2014), Stichel et al. (2012a,b), Zimmermann et al. (2009a,b). Data for sediments are from Bayon et al. (2009), Chen et al., (2012), Garcon et al., (2013). Data for Fe–Mn crusts are from Albarède et al. (1998), David et al. (2001).

4.2.3. LSW and IW

The depth of LSW formation is highly variable from year to year depending on the atmospheric conditions of the previous winter, such that colder conditions lead to more intense convection (Yashayaev and Clark, 2006; Yashayaev et al., 2008). As outlined in Section 2.2, a distinction can be made between SLSW (27.70 and 27.725 kg/m^3) and DLSW (27.75 and 27.79 kg/m^3) representing the remnants of the LSW that formed during the last cold state of the Labrador Sea between the late 1980's and the early 90's. This layer was also detected in 2008 as a layer of higher density and salinity below SLSW (Figs. 2 and 9) (Yashayaev et al., 2008).

The εNd signatures of SLSW and DLSW in our study are consistent with previously published data (Lacan and Jeandel, 2005; Lambelet et al., 2015) and reveal an average value of −14.1. There has only been one previous study reporting εHf signatures of two samples collected in the Labrador Sea (Rickli et al., 2009). The sample from a depth corresponding to SLSW (1000 m, εHf = −2.1) is within the range of values of SLSW along our transect (εHf ranges between −1.3 and −4.3). Unlike εNd, the εHf between 1700 and 2000 m is distinct from the upper water column, allowing DLSW and SLSW to be distinguished at each station. Deep LSW sampled at densities between 27.76 and 27.77 kg/m^3 at st. 17.5, 2000 m and st. 13.6, 1700 m, st. 15.5, 1700 m and st. 8.5, 1500 m has εHf signatures between −2.2 and −4.9. Less radiogenic values of DLSW at some stations in comparison to SLSW can be explained by a larger influence of IW, which has highly negative εHf values as recorded at st. 28 (εHf = −11.7) (Figs. 4 and 7). More radiogenic εHf signatures at st. 15.5, 1700 m and st. 8.5, 1500 m show values closer to the one recorded by SLSW, but the samples are lower in oxygen and more salty, which indicates the presence of DLSW and implies mixing between the two water masses. This is also explainable by the fact that this layer formed between 1980 and 1994 lost much of its distinct signature via mixing and most likely was not evenly distributed across the Labrador Sea (Yashayaev et al., 2008).

The more radiogenic εHf signatures in the upper column of ∼−1.3 at st. 17.5, 1000 m and ∼−1.9 at st. 15.5, 1000 m may be explained by the intrusion of SPMW, which has a more positive εHf signature of −1.6 and is characterized by a less radiogenic εNd signatures of −14.8 (Rickli et al., 2009). Less radiogenic εHf signatures at st. 13.6, 1000 m and st. 8.5, 1050 m and 750 m are best explained by the admixture of highly unradiogenic IW, which is consistent with much more radiogenic εHf signatures of surface waters at these stations (Fig. 7).

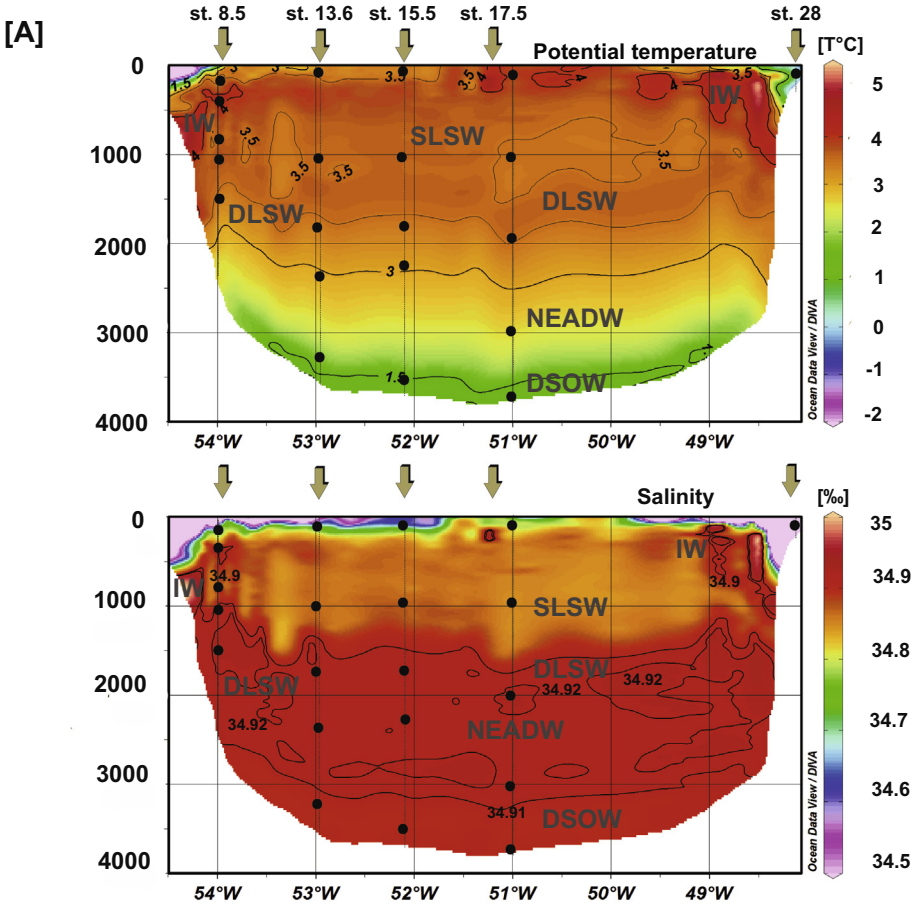

Fig. 9. Potential temperature (A) and salinity (B) versus depth across the AR7W transect in May, 2013. Contours denote potential temperatures and salinities of different water masses. Black dots represent the depths, from which water samples were taken at each station. Figure was created with ODV software (Schlitzer, 2015).

4.3. Upper water column

At st. 28, 100 m, the εHf signal is extremely unradiogenic at −11.7, which is the most negative value ever measured for Hf isotopes in seawater so far, while εNd signature of −15.7 is the same within the error as the surface waters across the Labrador Sea sampled at other stations. These waters are advected along the slope of the Labrador Sea. Their presence has not only been recorded in temperature, salinity and oxygen characteristics on the Canadian side of the Labrador Sea (Fig. 2, Fig. 9), but also in the Hf isotope signatures (Fig. 7). At st. 8.5, 400 m and even 13.6, 100 m, these waters are characterized by highly unradiogenic εHf signatures between −8.3 and −7.8, and εNd signatures ranging from −14.0 to −16.4. Admixture of these water masses causes εHf at stations 8.5 and 13.6 to be less radiogenic than εHf signatures prevailing at the corresponding depths at the central Labrador Sea stations. As we assume that this sample represents IW, its highly unradiogenic εHf and unradiogenic εNd signatures require discussion. Taking into account the origin and the flow path of IW and their potential close contact with basaltic rocks from Iceland, we would expect rather more radiogenic εHf and εNd signatures, likely similar to ISOW. This apparent conflict can be explained in a few ways: (i) the NAC waters are unradiogenic, which needs to be confirmed by direct measurements, (ii) there is no significant influence of the weathering of basaltic rocks on IW, (iii) there is a significant unradiogenic input from Greenland that shifts the signature. The latter explanation is favored due to higher REE and Nd concentration at st. 28 in comparison to the open Labrador Sea.

4.4. Extending the Nd/Hf isotope seawater array

On a plot of εHf against εNd, the seawater data of our study confirm the clear deviation from the terrestrial array, consistent with previous findings (e.g. Godfrey et al., 1997; Albarede et al., 1998; David et al., 2001; Rickli et al., 2009). In comparison to Fe–Mn crusts the new data show a larger range and significantly extend the seawater array at the unradiogenic end (up to −11 for εHf). The εHf and εNd isotopic signatures of Fe–Mn crusts recovered in the Atlantic Ocean from different depths (Piotrowski et al., 2000; David et al., 2001) are consistent with the combined εHf and εNd signatures from LSW, NEADW and DSOW in the Labrador Sea, which form the NADW. In addition, the two crusts Hudson st. 54 (~1829 m; εHf = +0.2, εNd = −12.9) and TR079 (~2000 m; εHf = 0, εNd = −12.5), as well as crust ALV 539 (~2700 m; εHf = −2.2, εNd = −12.9) (David et al., 2001) show the same trend observed along the Halifax line at st. HL08 and HL11, where these stations have an εNd like NADW, while with increasing depth εHf becomes less radiogenic.

Most of the new Labrador Sea data plot between the seawater and terrestrial arrays reflecting the degree of the incongruent weathering delivered to the source waters around the Labrador Sea (Fig. 8) (Bayon et al., 2006; Rickli et al., 2013). Most of the deep water and surface samples fall on the seawater array, suggesting that their signature reflects the true water mass signature of the dissolved hafnium fraction. However, samples representing LSW plot very close to the clay array recently derived by Bayon et al. (2016). This may suggest that intermediate waters in the Labrador Sea are largely controlled by Hf release from the dissolution of clay particles or the presence of very fine clay particles (<0.45 μm) or clay associated colloids in the water samples.

Interestingly, the samples that are under the strongest influence of terrestrial inputs, such as shallow Canadian shelf samples BIL02, BIL04, and BIL06, plot directly on or slightly above the seawater array and therefore reflect the strongest incongruent weathering signal at the lower end of the seawater array. The rapid change in Hf isotope signatures when moving away from the shore, accompanied by a decrease in Hf concentration in samples BIL04 and BIL06, suggests a high particle reactivity of Hf and fast removal from the surface waters. Samples collected at stations 28, 100 m and st. 8.5, 400 m plot well along the zircon free sediment array (Bayon et al., 2009). This supports our assumption that these waters are significantly influenced by terrestrial inputs from Greenland. Samples collected at st. HL11, characterized by a less radiogenic εHf signature, and at st. 15.5, 3512 m, also plot close to the zircon free sediment array, possibly indicating an input from resuspended sediments or an extensive nepheloid layer.

5. CONCLUSIONS

The first combined systematic investigation of the distributions of dissolved εNd and εHf signatures in the Labrador Sea in 2013 reveals distinct water mass signatures. The εHf signatures in the Labrador Sea allow distinction of particular water masses that do not differ in their Nd isotope compositions. This is the consequence of the large range of Hf isotope compositions of the weathering inputs from the adjacent continental landmasses combined with the likely shorter residence time of Hf than Nd in the Labrador Sea. The new data for intermediate waters fall along the new clay array, suggesting that these waters may be affected by dissolution of clay particles. Some of the samples fall along the zircon free sediment array, clearly supporting terrestrial input at these locations. The new data also significantly expand the unradiogenic end of the seawater array. The new data allow the application of Hf isotopes as a sensitive tracer of water mass mixing processes in the restricted Labrador Sea Basin and the detection of changes in the source waters feeding Labrador Sea Water production on decadal time scales. While tracing of large scale ocean mixing processes may not be possible based on Hf isotopes, there is clearly prospect for their application in other restricted basins with similar geological and hydrographic settings.

ACKNOWLEDGMENTS

Full-depth temperature, salinity and DO profiles and water samples, including Hf–Nd isotopes, on the AR7W (Atlantic Repeat Hydrography Line 7 West) line across the Labrador Sea and extended Halifax Line (XHL) were obtained during Fisheries and Oceans Canada's (DFO's) annual survey as part of its Atlantic

Zone Off-shelf Monitoring Program (AZOMP; http://www.bio.gc.ca/science/monitoring-monitorage/azomp-pmzao/azomp-pmzao-en.php). The Labrador Sea component of the AZOMP survey, generally conducted in spring shortly after the wintertime convection period, is a continuation of annual surveys of the AR7W line conducted by the Bedford Institute of Oceanography (BIO) since the start of the World Ocean Circulation Experiment (WOCE) in 1990 (e.g., Lazier et al., 2002; Yashayaev et al., 2015). Since 2004, the AR7W survey has been carried out in May occupied between the Labrador and Greenland Shelves.

A. Filippova was supported by a PhD fellowship of the Helmholtz Research School on Ocean System Science and Technology HOSST (www.hosst.org) at GEOMAR Helmholtz Centre for Ocean Research Kiel (VH-KO-601) and Kiel University. We thank Torben Stichel for discussions. We thank Philipp Böning for assistance with Nd measurements. We also would like to thank Tianyu Chen, Veit Dausmann, Jutta Heinze, Georgi Laukert, Anne Osborne, and Moritz Zieringer for their help in the laboratory. The crew of CCGS Hudson is thanked for their help during sampling on board. Financial support for the analyses in Oldenburg came from the ICBM, Oldenburg, and the Max Planck Institute for Marine Microbiology, Bremen.

REFERENCES

Albarède F., Simonetti A., Vervoort J. D., Blichert-Toft J. and Abouchami W. (1998) A Hf–Nd isotopic correlation in ferromanganese nodules. *Geophys. Res. Lett.* **25**(20), 3895–3898.

Andersson P., Dahlqvist R., Ingri J. and Gustafsson Ö. (2001) The isotopic composition of Nd in boreal river: a reflection of selective weathering and colloidal transport, 2001. *Geochim. Cosmochim. Acta* **65**, 521–527.

Arsouze T., Dutay J.-C., Lacan F. and Jeandel C. (2009) Reconstructing the Nd oceanic cycle using a coupled dynamical biogeochemical model. *Biogeosciences* **6**(12), 2829–2846.

Azetsu-Scott K., Jones E. P. and Yashayaev I. (2003) Time series study of CFC concentrations in the Labrador Sea during deep and shallow convection regimes (1991–2000). *J. Geophys. Res.* **108**(C11), 3354. http://dx.doi.org/10.1029/2002JC001317.

Barfod G. H., Otero O. and Albarède F. (2003) Phosphate Lu–Hf geochronology. *Chem. Geol.* **200**, 241–253.

Bayon G., Vigier N., Burton K. W., Brenot A., Carignan J. and Etoubleau J. (2006) The control of weathering processes on riverine and seawater hafnium isotope ratios. *Geology* **34**, 433–436.

Bayon G., Burton K. W., Soulet G., Vigier N., Dennielou B., Etoubleau J., Ponzevera E., German C. R. and Nesbitt R. W. (2009) Hf and Nd isotopes in marine sediments: constraints on global silicate weathering. *Earth Planet. Sci. Lett.* **277**, 318–326.

Bayon G., Skonieczny C., Delvigne C., Toucanne S., Bermell S., Ponzevera E. and André L. (2016) Environmental Hf–Nd isotopic decoupling in World river clays. *Earth Planet. Sci. Lett.* **438**, 25–36.

Bau M. and Koshinsky A. (2006) Hafnium and neodymium isotopes in seawater and in ferromanganese crusts: the "element perspective". *Earth Planet. Sci. Lett.* **241**, 952–961.

Blichert-Toft J. and Arndt N. T. (1999) Hf isotope compositions of komatiites. *Earth Planet. Sci. Lett.* **171**, 439–451. http://dx.doi.org/10.1016/S0012-821x(99)00151-X.

Bouvier A., Vervoort J. D. and Patchett P. J. (2008) The Lu–Hf and Sm–Nd isotopic composition of CHUR: constraints from unequilibrated chondrites and implications for the bulk composition of terrestrial planets. *Earth Planet. Sci. Lett.* **273**, 48–57. http://dx.doi.org/10.1016/j.epsl.2008.06.010.

Bruland K. W. (1983) Trace elements in sea water. In *Chemical Oceanography, 8* (eds. J. P. Riley and R. Chester). Academic Press, pp. 157–220.

Camire G. E., La Fleche M. R. and Jenner G. A. (1995) Geochemistry of Pre-Taconian Mafic Volcanism in the Humber zone of the Northern Appalachians, Quebec, Canada. *Chem. Geol.* **119**, 55–77. http://dx.doi.org/10.1016/0009-2541(94)00104-G.

Chen T. Y., Ling H. F., Frank M., Zhao K. D. and Jiang S. Y. (2011) Zircon effect alone insufficient to generate seawater Nd–Hf isotope relationships. *Geochem. Geophys. Geosyst.* **12**(5), Q05003. http://dx.doi.org/10.1029/2010GC003363, ISSN:1525-2027.

Chen T. Y., Frank M., Brian A. H., Gutjahr M. and Spielhagen R. F. (2012) Variations of North Atlantic inflow to the central Arctic Ocean over the last 14 million years inferred from hafnium and neodymium isotopes. *Earth Planet. Sci. Lett.* **353–354**, 82–92.

Chen T.-Y., Stumpf R., Frank M., Beldowski J. and Staubwasser M. (2013) Constraining geochemical cycling of hafnium and neodymium in the central Baltic Sea. *Geochim. Cosmochim. Acta* **123**, 166–180. http://dx.doi.org/10.1016/j.gca.2013.09.011.

Chekol T. A., Kobayashi K., Tetsuya Yokoyama., Sakaguchi C. and Nakamura E. (2011) Timescales of magma differentiation from basalt to andesite beneath Hekla Volcano, Iceland: constraints from U–series disequilibria in lavas from the last quarter-millennium flows. *Geochim. Cosmochim. Acta* **75**, 256–283.

Csanady G. T. (1976) Mean circulation in shallow seas. *J. Geophys. Res.* **81**, 5389–5399.

Csanady G. T. (1978) The arrested topographic wave. *J. Phys. Oceanogr.* **8**, 47–62.

David K., Frank M., O'Nions R. K., Belshaw N. S., Arden J. W. and Hein J. R. (2001) The Hf isotope composition of global seawater and the evolution of Hf isotopes in the deep Pacific Ocean from Fe–Mn crusts. *Chem. Geol.* **178**, 23–42.

Firdaus M. L., Norisuye K., Nakagawa Y., Nakatsuka S. and Sohrin Y. (2008) Dissolved and labile particulate Zr, Hf, Nb, Ta, Mo and W in the western North Pacific Ocean. *J. Oceanogr.* **64**, 247–257.

Firdaus M. L., Minami T., Norisuye K. and Sohrin Y. (2011) Strong elemental fractionation of Zr–Hf and Nb–Ta across the Pacific Ocean. *Nat. Geosci.* **4**, 227–230, 10 1038/ngeo1114.

Fitton J. G., Larsen L. M., Saunders A. D., Hardarson B. S. and Kempton P. D. J. (2000) Paleogene continental to oceanic magmatism on the SE Greenland continental margin at 63° N: a review of the results of ocean drilling program legs 152 and 163. *Petrology* **41**, 951–966. http://dx.doi.org/10.1093/petrology/41.7.951.

Fogelqvist E., Blindheim J., Tanhua T., Osterhus S., Buch E. and Rey F. (2003) Greenland-Scotland overflow studied by hydrochemical multivariate analysis. *Deep-Sea Res. I* **50**, 73–102.

Frank M. (2002) Radiogenic isotopes: tracers of past ocean circulation and erosional input. *Rev. Geophys.* **40**(1001), 1001. http://dx.doi.org/10.1029/2000RG000094.

Fröllje H., Pahnke K., Schnetger B., Brumsack H.-J., Dulai H. and Fitzsimmons J. N. (2016) Hawaiian imprint on dissolved Nd and Ra isotopes and rare earth elements in the central North Pacific: local survey and seasonal variability. *Geochim. Cosmochim. Acta* **189**, 110–131.

Gaffney A. M., Blichert-Toft J., Nelson B. K., Bizzarro M., Rosing M. T. and Albarede F. (2007) Constraints on source-forming processes of West Greenland kimberlites inferred from Hf–Nd isotope systematics. *Geochim. Cosmochim. Acta* **71**, 2820–2836. http://dx.doi.org/10.1016/j.gca.2007.03.009.

Garcon M., Chauvel C., France-Lanord C., Huyghe P. and Lave J. (2013) Continental sedimentary processes decouple Nd and Hf isotopes. *Geochim. Cosmochim. Acta* **121**, 177–195. http://dx.doi.org/10.1016/j.gca.2013.07.027.

Gerasimovsky V. I., Laktionova N. V. and Kovalenker V. G. (1975) Vanadium, chromium, nickel cobalt and copper in Iceland lavas. *Geochem. Int.* **12**(4), 160–171.

Godfrey L. V., White W. M. and Salters V. J. M. (1996) Dissolved zirconium and hafnium distributions across a shelf break in the northeastern Atlantic Ocean. *Geochim. Cosmochim. Acta* **60**, 3995–4006. http://dx.doi.org/10.1016/S0016-7037(96)00246-3.

Godfrey L. V., Lee D. C., Sangrey W. F., Halliday A. N., Salters V. J. M., Hein J. R. and White W. M. (1997) The Hf isotopic composition of ferromanganese nodules and crusts and hydrothermal manganese deposits: implications for seawater Hf. *Earth Planet. Sci. Lett.* **151**(1–2), 91–105.

Godfrey L. V., Zimmermann B., Lee D. C., King R. L., Vervoort J. D., Sherrell R. M. and Halliday A. N. (2009) Hafnium and neodymium isotope variations in NE Atlantic seawater. *Geochem. Geophys. Geosyst.* **10**, Q08015. http://dx.doi.org/10.1029/2009gc002508.

Goldstein S. L. and Hemming S. R. (2003) *Long-lived Isotopic Tracers in Oceanography, Paleoceanography and Ice-sheet Dynamics*, Book, Chapter 6.17.

Goldstein S. J. and Jacobsen S. B. (1988) REE in the Great River estuary, northwest Quebec. *Earth Planet. Sci. Lett.* **88**, 241–252.

Goldstein S. L., O'Nions R. K. and Hamilton P. J. (1984) A Sm–Nd isotopic study of atmospheric dust and particulates from major river systems. *Earth Planet. Sci. Lett.* **70**, 221–236.

Goodenough K. M., Upton B. G. J. and Ellam R. M. J. (2002) Long-term memory of subduction processes in the lithospheric mantle: evidence from the geochemistry of basic dykes in the Gardar Province of south Greenland. *Geol. Soc. London* **159**, 705–714. http://dx.doi.org/10.1144/0016-764901-154.

Grasse P., Stichel T., Stumpf R., Stramma L. and Frank M. (2012) The distribution of neodymium isotopes and concentrations in the Eastern Equatorial Pacific: water mass advection versus particle exchange. *Earth Planet. Sci. Lett.* **353–354**, 198–207.

Hathorne E. C., Haley B., Stichel T., Grasse P., Zienger M. and Frank M. (2012) Online preconcentration ICP-MS analysis of rare earth elements in seawater. *G*^{3} **13**(1), Q01020. http://dx.doi.org/10.1029/2011GC003907, ISSN:1525-2027.

Hathorne E. C., Stichel T., Brück B. and Frank M. (2015) Rare earth element distribution in the Atlantic sector of the Southern Ocean: the balance between particle scavenging and vertical supply. *Mar. Chem.* **177**(Part 1), 157–171.

Hoffmann J. E., Münker C., Polat A., König S., Mezger K. and Rosing M. T. (2010) Highly depleted hadean mantle reservoirs in the sources of early Archean arc-like rocks, Isua Supracrustal Belt, Southern West Greenland. *Geochim. Cosmochim. Acta* **74**, 7236–7260. http://dx.doi.org/10.1016/j.gca.2010.09.027.

Jackson M. G., Carlson R. W., Kurz M. D., Kempton P. D., Francis D. M. and Blusztajn J. (2010) Evidence for the survival of the oldest terrestrial mantle reservoir. *Nature* **466**, 853–856. http://dx.doi.org/10.1038/NATURE09287.

Jacobsen S. B. and Wasserburg G. J. (1980) Sm–Nd isotopic evolution of chondrites. *Earth Planet. Sci. Lett.* **50**, 139–155.

Kearns E. J. and Rossby H. T. (1998) Historical position of the North Atlantic Current. *J. Geophys. Res.* **103**, 15.509–15.524.

Kitagawa H., Kobayashi K., Makishima A. and Nakamura E. (2008) Multiple pulses of the mantle plume: evidence from tertiary Icelandic lavas. *J. Petrol.* **49**, 1365–1396.

Koornneef J. M., Stracke A., Bourdon B., Meier M. A., Jochum K. P., Stoll B. and Grönvold K. (2012) Melting of a two-component source beneath Iceland. *J. Petrol.* **53**, 127–157.

La Fleche M. R., Camire G. E. and Jenner G. A. (1998) Geochemistry of post-arcadian, carboniferous continental intraplate basalts from the Maritimes Basin, Magdalenen Islands, Quebec, Canada. *Chem. Geol.* **148**, 115–136. http://dx.doi.org/10.1016/S0009-2541(98)00002-3.

Lacan F. and Jeandel C. (2004a) Denmark Strait water circulation traced by heterogeneity in neodymium isotopic compositions. *Deep-Sea Res. I* **51**(1), 71–82. http://dx.doi.org/10.1016/j.dsr.2003.09.006.

Lacan F. and Jeandel C. (2004b) Neodymium isotopic composition and rare earth element concentrations in the deep and intermediate Nordic Seas: Constraints on the Iceland Scotland Overflow Water signature. *Geochem. Geophys. Geosyst.* **5**. http://dx.doi.org/10.1029/2004GC000742.

Lacan F. and Jeandel C. (2005) Acquisition of the neodymium isotopic composition of the North Atlantic Deep Water. *G*^{3} **6** (12), Q12008–15. http://dx.doi.org/10.1029/2005GC000956, ISSN:1525-2027.

Lacan F., Tachikawa K. and Jeandel C. (2012) Neodymium isotopic composition of the oceans: a compilation of seawater data. *Chem. Geol.* **300–301**, 177–184. http://dx.doi.org/10.1016/j.chemgeo.2012.01.019.

Lambelet M., van de Flierdt T., Crocket K., Rehkämper M., Kreissig K., Coles B., Rijkenberg M. J. A., Gerringa L. J. A., de Baar H. J. W. and Steinfeldt R. (2015) Neodymium isotopic composition and concentration in the western North Atlantic Ocean: results from the GEOTRACES GA02 section. *Geochim. Cosmochim. Acta* **177**, 1–29. http://dx.doi.org/10.1016/j.gca.2015.12.019.

Lazier J. R. N. and Wright D. G. (1993) Annual velocity variations in the Labrador Current. *J. Phys. Oceanogr.* **23**, 659–678.

Lazier J., Hendry R., Clarke A., Yashayaev I. and Rhines P. (2002) Convection and restratification in the Labrador Sea, 1990–2000. *Deep-Sea Res. I* **49**(10), 1819–1835. http://dx.doi.org/10.1016/S0967-0637(02)00064-X.

Maclachlan K. and Dunning G. R. (1998) 235–258 U–Pb ages and tectonomagmatic relationships of Early Ordovician Low-Ti Tholeiites, Boninites and related plutonic rocks in Central Newfoundland, Canada. *Contrib. Mineral. Petrol.* **133**.

Maclachlan K., Dunning G. R. and Can J. (1998) U–Pb ages and tectono-magmatic evolution of Middle Ordovician volcanic rocks of the Wild Bight Group, Newfoundland, Appalachians. *Earth Sci.* **35**, 998–1017. http://dx.doi.org/10.1139/cjes-35-9-998.

Manning C. J. and Thirlwall M. F. (2014) Isotopic evidence for interaction between Öraefajökull mantle and the eastern rift zone, Iceland. *Contrib. Mineral. Petrol.* **167**(959).

McKelvey B. A. and Orians K. J. (1998) The determination of dissolved zirconium and hafnium from seawater using isotope dilution coupled plasma mass spectrometry. *Mar. Chem.* **60**, 245–255.

McLennan S. M. (2001) Relationships between the trace element composition of sedimentary rocks and upper continental crust. *Geochem. Geophys. Geosyst.* **2**(4), 1–24. http://dx.doi.org/10.1029/2000GC000109.

Minifie M. J., Kerr A. C., Ernst R. E., Hastie A. R., Ciborowski T. J. R., Desharnais G. and Millar I. L. (2013) The Northern and Southern sections of the Western ca. 1880 Ma circum-superior Large Igneous Province, North America: the Pickle Crow Dyke connection? *Lithos* **174**, 217–235. http://dx.doi.org/10.1016/j.lithos.2012.03.017.

Münker C., Weyer S., Scherer S. and Mezger K. (2001) Separation of high field strength elements (Nb, Ta, Zr, Hf) and Lu from rock samples for MC-ICPMS measurements. *Geochem. Geophys. Geosyst.* **2**, 12. http://dx.doi.org/10.1029/2001GC000183.

Nowell G. M., Kempton P. D., Noble S. R., Fitton J. G., Saunders A. D., Mahoney J. J. and Taylor R. N. (1998) High precision Hf isotope measurements of MORB and OIB by thermal ionization mass spectrometry: insights into the depleted mantle. *Chem. Geol.* **149**, 211–233. http://dx.doi.org/10.1016/S0009-2541(98)00036-9.

Nozaki Y. and Alibo D. S. (2003) Importance of vertical geochemical processes in controlling the oceanic profiles of dissolved rare earth elements in the northeastern Indian Ocean. *Earth Planet. Sci. Lett.* **205**, 155–172.

Öhlander B., Ingri J., Land M. and Schöberg H. (2000) Change of Sm–Nd isotope composition during weathering of till. *Geochim. Cosmochim. Acta* **64**, 813–820.

Pahnke K., van de Flierdt T., Jones K. M., Lambelet M., Hemming S. R. and Goldstein S. L. (2012) GEOTRACES intercalibration of neodymium isotopes and rare earth element concentrations in seawater and suspended particles. Part 2: systematic tests and baseline profiles. *Limnol. Oceanogr.* **10**, 252–269.

Patchett P. J., White W. M., Feldman H., Kielinczuk S. and Hofmann A. W. (1984) Hafnium Rare-Earth element fractionation in the sedimentary system and crystal recycling into the earth's mantle. *Earth Planet. Sci. Lett.* **69**, 365–378.

Pearce C. R., Jones M. T., Oelkers E. H., Pradoux C. and Jeandel C. (2013) The effect of particulate dissolution on the neodymium (Nd) isotope and Rare Earth Element (REE) composition of seawater. *Earth Planet. Sci. Lett.* **369–370**, 138–147. http://dx.doi.org/10.1016/j.epsl.2013.03.023.

Peate D. W., Breddam K., Baker J. A., Kurz M. D., Barker A. K., Prestvik T., Grassineau N. and Skovgaard A. C. (2010) Compositional characteristics and spatial distribution of enriched Icelandic mantle components. *J. Petrol.* **51**, 1447–1475.

Pettke T. D., Lee D. C., Halliday A. N. and Rea D. K. (2002) Radiogenic Hf isotopic compositions of continental eolian dust from Asia, tis variability and its implications for seawater Hf. *Earth Planet. Sci. Lett.* **202**, 453–464. http://dx.doi.org/10.1016/S0012-821X(02)00778-1.

Piepgras D. J. and Wasserburg G. J. (1987) Rare-earth element transport in the western North Atlantic inferred from Nd isotopic observations. *Geochim. Cosmochim. Acta* **51**, 1257–1271. http://dx.doi.org/10.1016/j.epsl.2006.11.027.

Pin C. and Zalduegui J. S. (1997) Sequential separation of light rare-earth elements, thorium and uranium by miniaturized extraction chromatography: application to isotopic analyses of silicate rocks. *Anal. Chim. Acta* **339**, 79–89.

Piotrowski A. M., Lee D.-C., Christensen J. N., Burton K. W., Halliday A. N., Hein J. R. and Gunther D. (2000) Changes in erosion and ocean circulation recorded in the Hf isotopic compositions of North Atlantic and Indian Ocean ferromanganese crusts. *Earth Planet. Sci. Lett.* **181**, 315–325.

Piotrowski A. M., Goldstein S. L., Hemming S. R. and Fairbanks R. G. (2005) Temporal relationships of carbon cycling and ocean circulation at glacial boundaries. *Science* **307**, 1933–1938. http://dx.doi.org/10.1126/science.1104883.

Porcelli D., Andersson P. S., Baskaran M., Frank M., Björk G. and Semiletov I. (2009) The distribution of neodymium isotopes in Arctic Ocean basins. *Geochim. Cosmochim. Acta* **73**, 2645–2659. http://dx.doi.org/10.1016/j.gca.2008.11.046.

Rempfer J., Stocker T. F., Joos F., Dutay J.-C. and Sidall M. (2011) Modeling Nd-isotopes with a coarse resolution ocean circulation model: sensitivities to model parameters and source/sink distributions. *Geochim. Cosmochim. Acta* **75**, 5927–5950.

Reynaud T. H., Weaver A. J. and Greatbach R. J. (1995) Summer mean circulation of the northwestern Atlantic Ocean. *J. Geophys. Res.* **100**, 779–816.

Rickli J., Frank M. and Halliday A. N. (2009) The hafnium–neodymium isotopic composition of Atlantic seawater. *Earth Planet. Sci. Lett.* **280**, 118–127.

Rickli J., Frank M., Baker A. R., Aciego S., de Souza G., Georg R. B. and Halliday A. N. (2010) Hafnium and neodymium isotopes in surface waters of the eastern Atlantic Ocean: implications for sources and inputs of trace metals to the ocean. *Geochim. Cosmochim. Acta* **74**, 540–557.

Rickli J., Frank M., Stichel T., Georg R. B., Vance D. and Halliday A. N. (2013) Controls on the incongruent release of hafnium during weathering of metamorphic and sedimentary catchments. *Geochim. Cosmochim. Acta* **101**, 263–284. http://dx.doi.org/10.1016/j.gca.2012.10.019.

Rickli J., Gutjahr M., Vance D., Fisher-Gödde M., Hillenbrand C.-D. and Kuhn G. (2014) Neodymium and hafnium boundary contributions to seawater along the West Antarctic continental margin. *Earth Planet. Sci. Lett.* **394**, 99–110.

Rizo H., Boyet M., Blichert-Toft J. and Rosing M. T. (2013) Early mantle dynamics inferred from 142Nd variations in Archean rocks from southwest Greenland. *Earth Planet. Sci. Lett.* **377–378**, 324–335.

Rousseau T. C. C., Sonke J. E., Chmeleff J., van Beek P., Souhaut M., Boaventura G., Seyler P. and Jeandel C. (2015) Rapid neodymium release to marine waters from lithogenic sediments in the Amazon estuary. *Nat. Commun.*. http://dx.doi.org/10.1038/ncomms8592.

Salters V. J. M. and White W. M. (1998) Hf isotope constraints on mantle evolution. *Chem. Geol.* **145**, 447–460.

Schlitzer, R., Ocean Data View, odv.awi.de, 2015.

Schmitz W. (1996). , Technical report, WHOI-96-03.

Sholkovitz E. R. and Schneider D. L. (1991) Cerium redox cycles and rare earth elements in the Sargasso Sea. *Geochim. Cosmochim. Acta* **55**, 2737–2743.

Skulski T. and Percival J. A. (1996) Allochthonous 2.78 Ga oceanic plateau slivers in a 2.72 Ga Continental Arc sequence; Vizien Greenstone Belt, Northeastern Superior Province, Canada. *Lithos* **37**, 163–179. http://dx.doi.org/10.1016/0024-4937(95)00035-6.

Smith P. C. and Schwing F. B. (1990) Mean circulation and variability on the eastern Canadian continental shelf. *Cont. Shelf Res.* **11**, 977–1012.

Stern R. A., Percival J. A. and Mortensen J. K. (1994) Geochemical evolution of the Minto block: a 2.7 Ga continental magmatic arc built on the Superior Proto-Craton. *Precambrian Res.* **65**, 115–133. http://dx.doi.org/10.1016/0301-9268(94)90102-3.

Stichel T., Frank M., Rickli J., Hathorne E. C., Haley B., Jeandel C. and Pradoux C. (2012a) Sources and input mechanisms of hafnium and neodymium in surface waters of the Atlantic sector of the Southern Ocean. *Geochim. Cosmochim. Acta* **94**, 23–37.

Stichel T., Frank M., Rickli J. and Haley B. (2012b) The hafnium and neodymium isotope composition of seawater in the Atlantic sector of the Southern Ocean. *Earth Planet. Sci. Lett.* **317–318**, 282–294.

Stordal M. C. and Wasserburg G. J. (1986) Neodymium isotopic study of Baffin Bay water sources of REE from very old terranes. *Earth Planet. Sci. Lett.* **77**, 259–272.

Stracke A., Zindler A., Salters V. J. M., Mckenzie D. M., Blichert-Toft J., Albarede F. and Grönvold K. (2003) Theistareykir revisited. *Geochem. Geophys. Geosyst.* **4**.

Straneo F. and Saucier F. (2008) The outflow from Hudson Strait and its contribution to the Labrador Current. *Deep-Sea Res. I* **55**, 926–946.

Swinden H. S., Jenner G. A., Fryer B. J., Hertogen J. and Roddick J. C. (1990) Petrogenesis and paleotectonic history of the Wild

Bight Group, an Ordovician rifted island arc in Central Newfoundland. *Contrib. Mineral. Petrol.* **105**, 219–241. http://dx.doi.org/10.1007/BF00678987.

Szilas K., Hoffmann J. E., Schersten A., Rosing M. T., Windley B. F., Kokfelt T. F., Keulen N., Van Hinsberg V., Naeraa T., Frei R. and Münker C. (2012) Complex calc-alkaline volcanism recorded in mesoarchaean supracrustal belts north of Frederikshab Isblink, Southern West Greenland: implications for subduction zone processes in the early Earth. *Precambrian Res.* **208–211**, 90–123. http://dx.doi.org/10.1016/j.precamres.2012.03.013.

Szilas K., Hoffmann J. E., Schersten A., Kokfelt T. F. and Münker C. (2013) Archaean andesite petrogenesis: insights from the Graedefjord Supracrustal Belt, Southern West Greenland. *Precambrian Res.* **236**, 1–15. http://dx.doi.org/10.1016/j.precamres.2013.07.013.

Tanaka T., Togashi S., Kamioka H., Amakawa H., Kagami H., Hamamoto T., Yuhura M., Orihashi Y., Yoneda S., Shimizu H., Kunimaru T., Takahashi K., Yanagi T., Nakano T., Fujimaki H., Shinjo R., Asahara Y., Tanimizu M. and Dragusanu C. (2000) JNdi-1: a neodymium isotopic reference in consistency with LaJolla neodymium. *Chem. Geol.* **168**(3–4), 279–281.

Tappe S., Foley S. F., Kjarsgaard B. A., Romer R. L., Heaman L. M., Stracke A. and Jenner G. A. (2008) Between carbonatite and lamproite-diamondiferous torngat ultramafic lamprophyres formed by carbonate-fluxed melting of cratonic MARID-type metasomes. *Geochim. Cosmochim. Acta* **72**, 3258–3286. http://dx.doi.org/10.1016/j.gca.2008.03.008.

van de Flierdt T., Frank M., Lee D.-C. and Halliday A. N. (2002) Glacial weathering and the hafnium isotope composition of seawater. Earth Planet. Sci. Lett. 198, 167–175. Republished with corrections. *Earth Planet. Sci. Lett.* **201**, 639–647.

van de Flierdt T., Frank M., Lee D. C., Halliday A. N., Reynolds B. C. and Hein J. R. (2004a) New constraints on the sources and behavior of neodymium and hafnium in seawater from Pacific Ocean ferromanganese crusts. *Geochim. Cosmochim. Acta* **68**, 3827–3843.

van de Flierdt T., Frank M., Halliday A. N., Hein J. R., Hattendorf B., Gunther D. and Kubik P. W. (2004b) Tracing the history of submarine hydrothermal inputs and the significance of hydrothermal hafnium for the seawater budget- a combined Pb–Hf–Nd isotope approach. *Earth Planet. Sci. Lett.* **222**, 259–273.

van de Flierdt T., Goldstein S. L., Hemming S. R., Roy M., Frank M. and Halliday A. N. (2007) Global neodymium-hafnium isotope systematics- revisited. *Earth Planet. Sci. Lett.* **259**, 432–441.

van de Flierdt T. et al. (2012) GEOTRACES intercalibration of neodymium isotopes and rare earth element concentrations in seawater and suspended particles. Part 1: reproducibility of results for the international intercomparison. *Limnol. Oceanogr.* **10**, 234–251.

Vervoort J. D., Plank T. and Prytulak J. (2011) The Hf–Nd isotopic composition of marine sediments. *Geochim. Cosmochim. Acta* **75**(20), 5903–5926. http://dx.doi.org/10.1016/j.gca.2011.07.046.

West, Jr., D. P., Coish R. A. and Tomascak P. B. (2004) Tectonic setting and regional correlation of ordovician metavolcanic rocks of the Casco Bay Group, Maine: evidence from trace element and isotope geochemistry. *Geol. Mag.* **141**, 125–140. http://dx.doi.org/10.1017/S0016756803008562.

Wilson D. J., Piotrowski A. M., Galy A. and McCave I. N. (2012) A boundary exchange influence on deglacial neodymium isotope records from the deep western Indian Ocean. *Earth Planet. Sci. Lett.* **341–344**, 35–47.

Yashayaev I. (2007) Hydrographic changes in the Labrador Sea, 1960–2005. *Prog. Oceanogr.* **73**(3–4). http://dx.doi.org/10.1016/j.pocean.2007.04.015, 2442-276.

Yashayaev I. and Clark A. (2006) Recent warming of the Labrador Sea. *AZMP Bull. PMZA* **5**, 12–20.

Yashayaev I. and Dickson R. R. (2008) Transformation and fate of overflows in the northern North Atlantic. In *Arctic-Subarctic Ocean Fluxes: Defining the Role of the Northern Seas in Climate* (eds. R. R. Dickson, J. Meincke and P. Rhines). Springer, New York, pp. 505–526.

Yashayaev I. and Loder J. W. (2009) Enhanced production of Labrador Sea Water in 2008. *Geophys. Res. Lett.* **36**, L01606. http://dx.doi.org/10.1029/2008GL036162 (published online November 2008).

Yashayaev I. and Loder J. W. (2016) Recurrent replenishment of Labrador Sea water and associated decadal-scale variability. *J. Geophys. Res.*. http://dx.doi.org/10.1002/2016JC012046 (accepted manuscript).

Yashayaev I., Holliday N. P., Bersch M. and van Aken H. M. (2008) The Chapter 24: History of the labrador sea water: production, spreading, transformation and loss. In *Arctic-Subarctic Ocean Fluxes, Defining the Role of the Northern Seas in Climate* (eds. Bo Dickson, Jen Meincke and Pete Rhines). Springer, pp. 569–612.

Yashayaev I., Seidov D. and Demirov E. (2015) A new collective view of oceanography of the Arctic and North Atlantic basins. *Prog. Oceanogr.* **132**, 1–21.

Zimmermann B., Porcelli D., Frank M., Andersson P. S., Baskaran M., Lee D. C. and Halliday A. N. (2009a) Hafnium isotopes in Arctic Ocean water. *Geochim. Cosmochim. Acta* **73**, 32118–33233.

Zimmermann B., Porcelli D., Frank M., Rickli J., Lee D. C. and Halliday A. N. (2009b) The hafnium isotope composition of Pacific Ocean water. *Geochim. Cosmochim. Acta* **73**, 91–101.

Zindler A. and Komatiites E. G. (1982) *Nd and Sr Isotopic Studies of Komatiites and Related Rocks*. Allen & Unwin, pp. 399–420.

Associate editor: Tina van de Flierdt